Frontiers of Information Technology & Electronic Engineering
www.jzus.zju.edu.cn; engineering.cae.cn; www.springerlink.com
ISSN 2095-9184 (print); ISSN 2095-9230 (online)
E-mail: jzus@zju.edu.cn

A block-based secure and robust watermarking scheme for color images based on multi-resolution decomposition and de-correlation

Muhammad IMRAN‡[1], Bruce A. HARVEY[1], Muhammad ATIF[2], Adnan Ali MEMON[2]

[1]*Department of Electrical & Computer Engineering, Florida State University, Tallahassee 32306, USA*

[2]*Faculty of Information and Communication Technology, Balochistan University of Information Technology, Engineering and Management Sciences, Quetta 87100, Pakistan*

E-mail: mi14@my.fsu.edu; bharvey@fsu.edu; mohammad.atif@buitms.edu.pk; adnan.ali@buitms.edu.pk

Received Oct. 12, 2017; Revision accepted Mar. 16, 2018; Crosschecked July 3, 2019

Abstract: This paper presents a block-based secure and robust watermarking technique for color images based on multi-resolution decomposition and de-correlation. The principal objective of the presented scheme is to simultaneously meet all the four requirements (robustness, security, imperceptibility, and capacity) of a good watermarking scheme. The contribution of this study is to basically achieve the four contradictory requirements that a good watermarking scheme must meet. To do so, different approaches are combined in a way that the four requirements are achieved. For instance, to obtain imperceptibility, the three color channels (red, green, and blue) are de-correlated using principal component analysis, and the first principal component (de-correlated red channel) is chosen for watermark embedding. Afterwards, to achieve robustness, the de-correlated channel is decomposed using a discrete wavelet transform (DWT), and the approximate band (the other three bands are kept intact to preserve the edge information) is further decomposed into distinct blocks. The random blocks are chosen based on a random generated key. The random selected blocks are further broken down into singular values and vectors. Based on the mutual dependency on singular values and vectors' matrices, the values are modified depending on the watermarking bits, and their locations are saved and used as another key, required when the watermark is to be extracted. Consequently, two-level authentication levels ensure the security, and using both singular values and vectors increases the capacity of the presented scheme. Moreover, the involvement of both left and right singular vectors along with singular values in the watermarking embedding process strengthens the robustness of the proposed scheme. Finally, to compare the presented scheme with the state-of-the-art schemes in terms of imperceptibility (peak signal-to-noise ratio and structural similarity index), security (with numerous fake keys), robustness (normalized correlation and bit error rate), and capacity, the Gonzalez and Kodak datasets are used. The comparison shows significant improvement of the proposed scheme over existing schemes.

Key words: Copyright protection; Data hiding; Multi-resolution decomposition; De-correlation; Security
https://doi.org/10.1631/FITEE.1700667 **CLC number:** TP391.4

1 Introduction

With the advent and rapid development of the World Wide Web and the ease of access to the Internet, multimedia data, such as images, audios, and videos, can be easily accessed, downloaded, copied, modified, and redistributed. On the one hand, this

‡ Corresponding author
ORCID: Muhammad IMRAN, http://orcid.org/0000-0002-1147-3159

provides a way to access useful information from anywhere instantly and easily; on the other hand, it has created problems for intellectual property owners. For instance, the data can be illegally copied and redistributed without any visible difference between the original and copied data, especially for an end user. It is also difficult to track the origin of illegal distribution of the copied material. Because of this illicit distribution, industries suffer from enormous loss each year (Tarisha, 2017). Therefore, some measures must be taken to avoid further unlawful distribution or to provide a method to claim ownership. To address these issues, watermarking is proposed as a prominent solution (Luo et al., 2010; You et al., 2010; Roy et al., 2015; Zong et al., 2015; Fazli and Moeini, 2016; Chang and Shen, 2017).

Image watermarking is a way of concealing information (watermark) that may be a logo or picture, into an image (host), which is to be secured (Chang and Shen, 2017). A watermarking technique must meet four challenges, capacity, robustness, security, and imperceptibility, to be efficient in terms of providing copyright protection (Kalantari et al., 2010; Makbool and Khoo, 2014; Zong et al., 2015).

Both spatial domain watermarking and transformed domain watermarking are available in the literature (Kalantari et al., 2010; You et al., 2010; Sadreazami and Amini, 2012; Ali and Ahn, 2014; Sadreazami et al., 2015; Amini et al., 2017b, 2017c). In the former watermarking technique, the host image is modified directly to embed the watermark (Kalantari et al., 2010; You et al., 2010). Many watermarking techniques in the spatial domain have been proposed (Chou and Liu, 2010; Luo et al., 2010). In the study of transform domain watermarking, the discrete Fourier (Hernandez et al., 2005; Chen et al., 2014), wavelet transform (Ali and Ahn, 2014; Amini et al., 2017a), contourlet transform (Ranjbara et al., 2013; Prathap et al., 2014), and some other transforms (Kalantari et al., 2010; You et al., 2010; Sadreazami and Amini, 2012) are applied to the host images, and then the watermark is embedded in the transform domain. Then the watermarked image is obtained by applying the inverse transform. The watermarking schemes in the spatial domain are simpler but more fragile compared to their counterparts (Hernandez et al., 2005; Kalantari et al., 2010; Ali and Ahn, 2014; Prathap et al., 2014).

In the literature, watermarking techniques for both gray-scale (Kalantari et al., 2010; Makbool and Khoo, 2014) and color images (Ranjbara et al., 2013; Prathap et al., 2014; Sadreazami et al., 2015; Amini et al., 2017c) are available. The watermarking techniques for color images have to face one additional challenge compared to gray-scale watermarking schemes. The extra constraint is that the color-channels of a color image are extremely correlated (Meylan and Ssstrunk, 2006; Drew and Bergner, 2008). A slight modification of any one of the three color channels results in significant change in the other two, which in turn results in overall deterioration of the visual quality of the original image. However, if these channels are uncorrelated, then modifying one channel will not affect other channels and imperceptibility will not be affected. To overcome this challenge, researchers have adopted different approaches. For instance, some have used luminance-in-quadrature-phase (YIQ) color space (Su et al., 2013), some have used luminance-chrominance-chroma (YUV) (Chou and Liu, 2010; Lina et al., 2010) in their techniques, and a few have opted for principal component analysis (PCA) (Prathap et al., 2014) to un-correlate the three channels. In the proposed technique, the three channels of a color image are uncorrelated using PCA. The use of PCA has improved the imperceptibility of watermarked images as shown in Section 3.1.

Another mathematical tool that has been frequently used in the field of image watermarking is singular value decomposition (SVD). There are certain properties of SVD: (1) Alteration in singular values does not degrade the original image's visual quality significantly (the same is true otherwise); (2) Singular values and vectors possess luminance and geometric information, respectively (Makbool and Khoo, 2014), which make them useful in watermarking (Liu and Tan, 2002; Lai, 2011a; Makbool and Khoo, 2014). Though using SVDs gives satisfactory results as far as robustness is concerned, it is inefficient in ensuring security (the watermarking technique must be able to reject all attempts to retrieve the watermark using incorrect keys) (Makbool and Khoo, 2014). For example, Liu and Tan (2002) proposed a spatial watermarking technique. The watermark is embedded by changing singular values of the host image, whereas the singular vectors are left unchanged. The singular vectors are saved as a security

key and required at the time of watermark retrieval. Later on, it was discovered that using altogether different singular vectors leads to a different watermark retrieval, which is not even embedded in that image (Zhang and Li, 2005; Rykaczewski, 2007). This means anyone with an incorrect key can extract the watermark of their choice, and hence can claim the ownership. Due to this major drawback, the principal purpose of a watermarking technique to ensure copyright protection cannot be achieved. An improved version of Liu and Tan (2002)'s technique was presented by Lai and Tsai (2010), using discrete wavelet transform (DWT) in addition to SVD. Nevertheless, the flaw in Liu and Tan (2002) was also presented in Lai and Tsai (2010). A slightly modified technique (Lai, 2011a) also had these kinds of flaws (Loukhaoukha, 2013; Yavuz and Telatar, 2013). Therefore, to design the proposed technique, importance is given to security, and it is confirmed that without an authentic key neither a true nor a fallacious watermark can be extracted, as shown in Section 3.4. The proposed scheme relies mainly on SVD. Therefore, the SVD-based techniques in Roy et al. (2015) and Fazli and Moeini (2016), which have also tried to meet the security requirement, are chosen for comparison. In addition, two more watermarking techniques in Han et al. (2017) and Vo et al. (2017), in which solutions have been proposed for color images, are also considered for comparison, especially in terms of imperceptibility. In addition to PCA and DWT, SVD is used in the proposed technique to achieve robustness and security. The proposed scheme relies mainly on DWT, SVD, and PCA, so these three mathematical tools are briefly discussed in the following subsections.

1.1 Discrete wavelet transform

The Fourier transform is a useful tool to analyze the frequency component of a signal, but it does not provide time information. However, the short time Fourier transform (STFT) provides information for both frequency and time of a signal. The length of the window is used to calculate spectrogram is limited, and hence it provides very limited frequency resolution.

To analyze the time and frequency information of a signal at the same time, wavelet transform is used (Gonzalez and Woods, 2008). Fig. 1 explains this phenomenon. DWT decomposes images of size $M \times N$ into approximate horizontal, vertical, and diagonal bands, each of size $(M/m) \times (N/m)$, where m represents the level of decomposition. DWT gives multi-resolution representation of an image (You et al., 2010). The high frequency bands (horizontal, vertical, and diagonal) represent the texture and edges of an image.

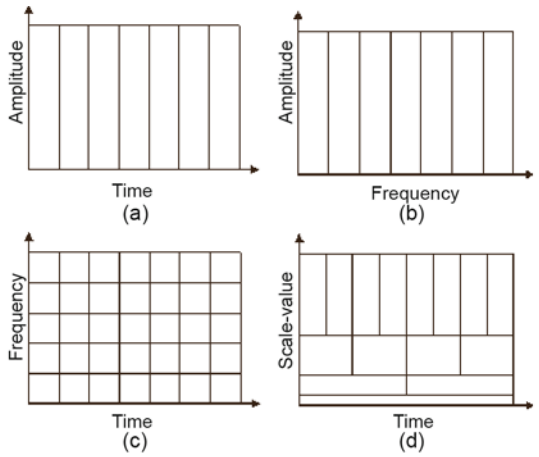

Fig. 1 Generic signal transform: (a) time domain; (b) frequency domain; (c) short time Fourier transform; (d) discrete wavelet transform

1.1.1 One-dimensional discrete wavelet transform

Let $f(n)$ represent a one-dimensional discrete signal of length M. Given the scaling function $\varphi_{j_0,k}$ and wavelet function $\Psi_{j,k}$, wavelet transform can be calculated as

$$W_\varphi(j_0,k) = \frac{1}{\sqrt{M}} \sum_{n=0}^{M} f(n)\varphi_{j_0,k}(n), \tag{1}$$

$$W_\Psi(j,k) = \frac{1}{\sqrt{M}} \sum_{n=0}^{M} f(n)\Psi_{j,k}(n), \tag{2}$$

where $j \geq j_0$, W_φ represents the approximation coefficient, and φ denotes detailed coefficients. Usually, $j_0 = 0$, $J = \log_2 M$, $n = 0, 1, \ldots, M-1$, $j = 0, 1, \ldots, J-1$, and $k = 0, 1, \ldots, 2^j - 1$. The signal $f(n)$ can be represented as a weighted sum of approximation and detailed coefficients:

$$\begin{aligned} f(n) = &\frac{1}{\sqrt{M}} \sum_k W_\varphi(j_0,k)\varphi_{j_0,k}(n) \\ &+ \frac{1}{\sqrt{M}} \sum_{j=j_0}^{\infty} \sum_k W_\Psi(j,k)\Psi_{j,k}(n). \end{aligned} \tag{3}$$

1.1.2 Two-dimensional discrete wavelet transform

Given an image $f(x,y)$ of size $M \times N$, the approximation and detailed coefficients are calculated as

$$W_\varphi(j_0,m,n)=\frac{1}{\sqrt{MN}}\sum_{x=0}^{M-1}\sum_{y=0}^{N-1}f(x,y)\varphi_{j_0,m,n}(x,y), \quad (4)$$

$$W_\Psi^i(j,m,n)=\frac{1}{\sqrt{MN}}\sum_{x=0}^{M-1}\sum_{y=0}^{N-1}f(x,y)\Psi_{j,m,n}^i(x,y), \quad (5)$$

where $i=\{\mathrm{H},\mathrm{V},\mathrm{D}\}$. $W_\varphi(j_0,m,n)$ represents the approximation coefficient of image $f(x,y)$ at the j_0 level. The detailed coefficients $W_\Psi^{\mathrm{H}}(j,m,n)$, $W_\Psi^{\mathrm{V}}(j,m,n)$, and $W_\Psi^{\mathrm{D}}(j,m,n)$ measure the variation along horizontal (x-axis), vertical (y-axis), and diagonal of a two-dimensional signal for $j \geq j_0$, respectively. Supposing $j_0=0$, $m=0,1,\ldots,M-1$, and $n=0,1,\ldots,N-1$, normally M and N are selected to be the same, so $J=\log_2 M$ and $J=\log_2 N$, $j=0,1,\ldots,J-1$. The scaling function $\varphi(x,y)$ and wavelet functions (directionally sensitive) $\Psi^{\mathrm{H}}(j,m,n)$, $\Psi^{\mathrm{V}}(j,m,n)$, and $\Psi^{\mathrm{D}}(j,m,n)$ are separable. Hence, they can be written as

$$\begin{cases}\varphi(x,y)=\varphi(x)\varphi(y),\\ \Psi^{\mathrm{H}}(x,y)=\Psi(x)\varphi(y),\\ \Psi^{\mathrm{V}}(x,y)=\varphi(x)\Psi(y),\\ \Psi^{\mathrm{D}}(x,y)=\Psi(x)\Psi(y).\end{cases} \quad (6)$$

Similarly, the image $f(x,y)$ can be represented as a weighted sum of approximation and detailed coefficients:

$$f(x,y)=\sqrt{\frac{1}{MN}}\Bigg(\sum_{m=0}^{M-1}\sum_{n=0}^{N-1}W_\varphi(j_0,m,n)\varphi_{j_0,m,n}(x,y) + \sum_{i=\mathrm{H},\mathrm{V},\mathrm{D}}\sum_{j=j_0}^{\infty}\sum_{m=0}^{M-1}\sum_{n=0}^{N-1}W_\Psi^i(j,m,n)\Psi_{j,m,n}^i(x,y)\Bigg). \quad (7)$$

The procedures of DWT and inverse discrete wavelet transform (IDWT) are shown in Figs. 2 and 3, respectively. Fig. 4 shows the original image and its DWT decomposed bands.

The approximation band shown in Fig. 4b can further be decomposed, and the size of next decomposed bands would be half the size of the approximation band. The further decomposed bands are shown in Fig. 5.

There are many advantages of using DWT, specifically in watermarking. For instance, DWT is very useful in image watermarking because it provides information regarding the area, and the

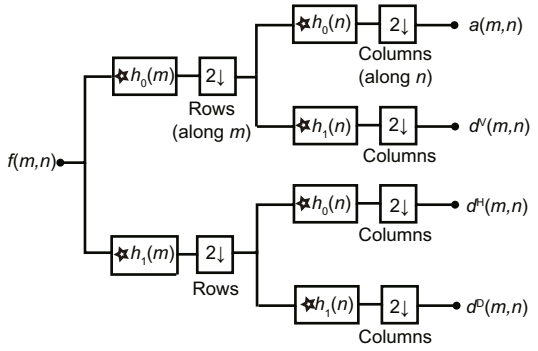

Fig. 2 Analysis filter bank (Gonzalez and Woods, 2008)

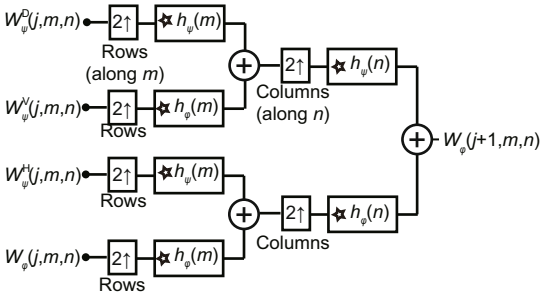

Fig. 3 Synthesis filter bank (Gonzalez and Woods, 2008)

Fig. 4 One-level DWT decomposition: (a) original image of size $M \times N$; (b) approximation band of size $(M/2) \times (N/2)$; (c) horizontal band of size $(M/2) \times (N/2)$; (d) vertical band of size $(M/2) \times (N/2)$; (e) diagonal band of size $(M/2) \times (N/2)$

Fig. 5 Two-level DWT decomposition: (a) approximation band from Fig. 4b; (b) approximation band of size $(M/4) \times (N/4)$; (c) horizontal band of size $(M/4) \times (N/4)$; (d) vertical band of size $(M/4) \times (N/4)$; (e) diagonal band of size $(M/4) \times (N/4)$

information is less sensitive to disturbances (Barni et al., 2001). Additionally, the three detailed subbands (horizontal, vertical, and diagonal bands) are not suitable for watermark embedding in terms of robustness, especially against compression or blurring (Barni et al., 2001).

1.2 Singular value decomposition

Given an image $\boldsymbol{A}$ of size $M \times N$, the singular value decomposition (SVD) is represented as

$$\boldsymbol{A} = \boldsymbol{U}\boldsymbol{S}\boldsymbol{V}^{\mathrm{T}}, \tag{8}$$

$$\boldsymbol{A} = \begin{bmatrix} a_{11} & a_{12} & \dots & a_{1N} \\ a_{21} & a_{22} & \dots & a_{2N} \\ \vdots & \vdots & & \vdots \\ a_{M1} & a_{M2} & \dots & a_{MN} \end{bmatrix}, \boldsymbol{U} = \begin{bmatrix} u_{11} & u_{12} & \dots & u_{1M} \\ u_{21} & u_{22} & \dots & u_{2M} \\ \vdots & \vdots & & \vdots \\ u_{M1} & u_{M2} & \dots & u_{MM} \end{bmatrix},$$

$$\boldsymbol{V} = \begin{bmatrix} v_{11} & v_{12} & \dots & v_{1N} \\ v_{21} & v_{22} & \dots & v_{2N} \\ \vdots & \vdots & & \vdots \\ v_{N1} & v_{N2} & \dots & v_{NN} \end{bmatrix}, \boldsymbol{S} = \begin{bmatrix} s_{11} & s_{12} & \dots & s_{1N} \\ s_{21} & s_{22} & \dots & s_{2N} \\ \vdots & \vdots & & \vdots \\ s_{M1} & s_{M2} & \dots & s_{MN} \end{bmatrix},$$

where $\boldsymbol{U}$ is an $M \times M$ unitary matrix, and the M columns of $\boldsymbol{U}$ are called left singular vectors and contain geometrical details of an image, specifically the horizontal details. $\boldsymbol{S}$ is an $M \times N$ diagonal matrix containing non-negative values called singular values in descending order, containing the luminance information of an image. $\boldsymbol{V}$ is an $N \times N$ unitary matrix. The N columns of $\boldsymbol{V}$ are called right singular vectors and contain the vertical details of an image.

SVD has certain properties, which make it useful in the field of image processing like compression, watermarking, and noise reduction. A few of these properties are listed below: (1) The changes in singular values do not make any significant change in the image itself (Makbool and Khoo, 2014); (2) Singular values contain luminance information of an image (Makbool and Khoo, 2014); (3) Singular vectors $\boldsymbol{U}$ and $\boldsymbol{V}$ contain geometrical information (Makbool and Khoo, 2014), with $\boldsymbol{U}$ containing horizontal details of an image and $\boldsymbol{V}$ maintaining vertical details; (4) Singular values are arranged in descending order, with the highest singular value containing the most significant information and smaller values having less significant information. Thereby, smaller values can be neglected to save space, because their removals or changes have no significant impact on image quality (Makbool and Khoo, 2014).

1.3 Principal component analysis

PCA is used to represent observations, such as speech signals, images, and any general data, in a mutually independent form, which reduces the mutual dependencies of components in data (Mudrová and Procházka, 2005). For a given matrix $\boldsymbol{X}$ of size $N \times K$,

$$\begin{aligned} \boldsymbol{X} &= \begin{bmatrix} \boldsymbol{X}_1 & \boldsymbol{X}_2 & \dots & \boldsymbol{X}_n & \dots & \boldsymbol{X}_N \end{bmatrix}^{\mathrm{T}} \\ &= \begin{bmatrix} x_{11} & x_{12} & \dots & x_{1k} & \dots & x_{1K} \\ x_{21} & x_{22} & \dots & x_{2k} & \dots & x_{2K} \\ \vdots & \vdots & & \vdots & & \vdots \\ x_{n1} & x_{n2} & \dots & x_{nk} & \dots & x_{nK} \\ \vdots & \vdots & & \vdots & & \vdots \\ x_{N1} & x_{N2} & \dots & x_{Nk} & \dots & x_{NK} \end{bmatrix}, \end{aligned} \tag{9}$$

the principal components (mutually independent components) are obtained as follows:

$$\boldsymbol{Y} = \boldsymbol{V}(\boldsymbol{X} - \boldsymbol{M}_X), \tag{10}$$

where $\boldsymbol{M}_X$ is the mean value and is calculated using the following relationship:

$$\boldsymbol{M}_X = \frac{1}{K}\sum_{k=1}^{K} \boldsymbol{X}_n. \tag{11}$$

The vector $\boldsymbol{V}$ in Eq. (10) contains the eigenvectors of covariance matrix ($\boldsymbol{C}_X$) with respect to the corresponding eigenvalues, arranged in descending order. The covariance matrix is calculated as

$$\boldsymbol{C}_X = \frac{1}{K}\sum_{k=1}^{K} \boldsymbol{X}_n \boldsymbol{X}_n^{\mathrm{T}} - \boldsymbol{M}_X \boldsymbol{M}_X{}^{\mathrm{T}}. \tag{12}$$

PCA is a statistical technique with numerous applications such as data compression, decorrelation, and pattern recognition (Mudrová and Procházka, 2005; Santhi and Thangavelu, 2009; Gunjal and Mali, 2011). Since the three channels of a color image are extremely correlated (Santhi and Thangavelu, 2009; Bhagyashri and Joshi, 2011; Gunjal and Mali, 2011), modifying any one of them results in changes in the other two channels, which in turn degrades the visual quality of the image. Nonetheless, if these mutually dependent channels are de-correlated using PCA (Mudrová and Procházka, 2005; Sun and Bo, 2011), this dependency can be circumvented.

The detailed procedure of watermark embedding and extraction is discussed in a subsequent section.

2 Proposed scheme

In the presented secure and robust image watermarking scheme for color images, PCA is used to de-correlate the extremely mutually dependent color channels. Since the first principal component possesses nearly all information (Vidal et al., 2005), to embed a watermark, the first principal component is chosen. The principal component with maximum information is subjected to multi-resolution decomposition using DWT and results in four bands: $\mathbb{A}$, $\mathbb{H}$, $\mathbb{V}$, and $\mathbb{D}$. The approximation band $\mathbb{A}$ is chosen for watermark embedding, while keeping other bands intact to maintain the edge information of the image, as $\mathbb{H}$, $\mathbb{V}$, and $\mathbb{D}$ bands contain horizontal, vertical, and diagonal details, respectively. DWT not only improves the imperceptibility but also increases the security level because of the spreading of hidden information over the whole image during inverse transform. To ensure the security of the proposed scheme, $\mathbb{A}$ is further divided into distinct blocks. Then each block is decomposed into singular vectors ($\boldsymbol{U}$ and $\boldsymbol{V}$) and singular values (λ). Finally, the least correlated elements from $\boldsymbol{U}$, $\boldsymbol{V}$, and λ are selected for modification, and their locations are saved. Those locations work as a secret key and are required when the watermark is to be extracted. As a result, a watermarking technique for color images is devised to meet all four requirements (imperceptibility, security, robustness, and capacity) at the same time. The only limitation of the proposed scheme is that the size of watermark should be 1/64 of the size of the cover image. The detailed procedures of watermark embedding and extraction are discussed in Sections 2.1 and 2.2, respectively.

2.1 Watermark embedding

Three channels are extracted from the original color image $\boldsymbol{I}$ of size $M\times N$ as

$$\boldsymbol{I}_{\mathrm{R}}=\begin{bmatrix}\rho_{11} & \rho_{12} & \cdots & \rho_{1N}\\ \rho_{21} & \rho_{22} & \cdots & \rho_{2N}\\ \vdots & \vdots & & \vdots\\ \rho_{M1} & \rho_{M2} & \cdots & \rho_{MN}\end{bmatrix},\boldsymbol{I}_{\mathrm{G}}=\begin{bmatrix}\gamma_{11} & \gamma_{12} & \cdots & \gamma_{1N}\\ \gamma_{21} & \gamma_{22} & \cdots & \gamma_{2N}\\ \vdots & \vdots & & \vdots\\ \gamma_{M1} & \gamma_{M2} & \cdots & \gamma_{MN}\end{bmatrix},$$

$$\boldsymbol{I}_{\mathrm{B}}=\begin{bmatrix}\beta_{11} & \beta_{12} & \cdots & \beta_{1N}\\ \beta_{21} & \beta_{22} & \cdots & \beta_{2N}\\ \vdots & \vdots & & \vdots\\ \beta_{M1} & \beta_{M2} & \cdots & \beta_{MN}\end{bmatrix}. \tag{13}$$

A correlation matrix $\boldsymbol{C}$ for a given matrix $\boldsymbol{A}$ is calculated as

$$\begin{cases}\boldsymbol{C}=\dfrac{1}{M\times N}\boldsymbol{A}\boldsymbol{A}^{\mathrm{T}}=\boldsymbol{\Phi}\wedge\boldsymbol{\Phi}^{-1},\\ \boldsymbol{A}=\begin{bmatrix}\boldsymbol{\rho}_1 & \boldsymbol{\rho}_2 & \cdots & \boldsymbol{\rho}_i & \cdots & \boldsymbol{\rho}_M\\ \boldsymbol{\gamma}_1 & \boldsymbol{\gamma}_2 & \cdots & \boldsymbol{\gamma}_i & \cdots & \boldsymbol{\gamma}_M\\ \boldsymbol{\beta}_1 & \boldsymbol{\beta}_2 & \cdots & \boldsymbol{\beta}_i & \cdots & \boldsymbol{\beta}_M\end{bmatrix},\\ \boldsymbol{\Phi}=\begin{bmatrix}\phi_{11} & \phi_{12} & \phi_{13}\\ \phi_{21} & \phi_{22} & \phi_{23}\\ \phi_{31} & \phi_{32} & \phi_{33}\end{bmatrix},\\ \wedge=\begin{bmatrix}\wedge_{11} & 0 & 0\\ 0 & \wedge_{22} & 0\\ 0 & 0 & \wedge_{33}\end{bmatrix},\end{cases} \tag{14}$$

where $\boldsymbol{\rho}_i=[\rho_{i1},\rho_{i2},\ldots,\rho_{iN}]$, $\boldsymbol{\gamma}_i=[\gamma_{i1},\gamma_{i2},\ldots,\gamma_{iN}]$, $\boldsymbol{\beta}_i=[\beta_{i1},\beta_{i2},\ldots,\beta_{iN}]$, and $\wedge_{11}\geq\wedge_{22}\geq\wedge_{33}$.

PCA (disscused in Section 1.3) is used to obtain the de-correlated principal component, which is the red channel of matrix $\boldsymbol{C}$ (Vidal et al., 2005):

$$\begin{aligned}\boldsymbol{P}=\boldsymbol{\Phi}^{\mathrm{T}}\boldsymbol{A}&=\begin{bmatrix}\boldsymbol{P}_{\boldsymbol{\rho}} & \boldsymbol{P}_{\boldsymbol{\gamma}} & \boldsymbol{P}_{\boldsymbol{\beta}}\end{bmatrix}^{\mathrm{T}}\\ &=\begin{bmatrix}\boldsymbol{P}_{\boldsymbol{\rho}_1} & \boldsymbol{P}_{\boldsymbol{\rho}_2} & \cdots & \boldsymbol{P}_{\boldsymbol{\rho}_i} & \cdots & \boldsymbol{P}_{\boldsymbol{\rho}_M}\\ \boldsymbol{P}_{\boldsymbol{\gamma}_1} & \boldsymbol{P}_{\boldsymbol{\gamma}_2} & \cdots & \boldsymbol{P}_{\boldsymbol{\gamma}_i} & \cdots & \boldsymbol{P}_{\boldsymbol{\gamma}_M}\\ \boldsymbol{P}_{\boldsymbol{\beta}_1} & \boldsymbol{P}_{\boldsymbol{\beta}_2} & \cdots & \boldsymbol{P}_{\boldsymbol{\beta}_i} & \cdots & \boldsymbol{P}_{\boldsymbol{\beta}_M}\end{bmatrix},\end{aligned} \tag{15}$$

where $\boldsymbol{P}_{\boldsymbol{\rho}_i}=[p_{\rho_{i1}},p_{\rho_{i2}},\ldots,p_{\rho_{iN}}]$, $\boldsymbol{P}_{\boldsymbol{\gamma}_i}=[p_{\gamma_{i1}},p_{\gamma_{i2}},\ldots,p_{\gamma_{iN}}]$, and $\boldsymbol{P}_{\boldsymbol{\beta}_i}=[p_{\beta_{i1}},p_{\beta_{i2}},\ldots,p_{\beta_{iN}}]$.

Remark 1 Since the three channels of a color image are extremely correlated (Santhi and Thangavelu, 2009; Bhagyashri and Joshi, 2011; Gunjal and Mali, 2011), modifying any one of them results in changes in the other two channels, which in turn degrades the visual quality of the image. Nonetheless, if these mutually dependent channels are de-correlated using PCA (Sun and Bo, 2011), this dependency can be circumvented.

$\boldsymbol{P}_{\boldsymbol{\rho}}$ of $\boldsymbol{P}$ is used to obtain $\boldsymbol{P}_{\boldsymbol{\rho}\mathrm{n}}$:

$$\boldsymbol{P}_{\boldsymbol{\rho}\mathrm{n}}=\begin{bmatrix}p_{\rho_{11}} & p_{\rho_{12}} & \cdots & p_{\rho_{1N}}\\ p_{\rho_{21}} & p_{\rho_{22}} & \cdots & p_{\rho_{2N}}\\ \vdots & \vdots & & \vdots\\ p_{\rho_{M1}} & p_{\rho_{M2}} & \cdots & p_{\rho_{MN}}\end{bmatrix}. \tag{16}$$

$\boldsymbol{P}_{\boldsymbol{\rho}\mathrm{n}}$ is subjected to multi-resolution decomposition. We can obtain $\mathbb{A}$, $\mathbb{H}$, $\mathbb{V}$, and $\mathbb{D}$ bands using DWT:

$$(\mathbb{A},\mathbb{H},\mathbb{V},\mathbb{D})=\mathrm{DWT}(\boldsymbol{P}_{\boldsymbol{\rho}\mathrm{n}}). \tag{17}$$

Remark 2 DWT is used to improve robustness and security (Dharwadkar et al., 2011). During

the inverse transform, the embedding information is spread over the entire image, which improves robustness and security. From the four bands, the approximation band $\mathbb{A}$ is chosen for watermark embedding to keep the edge information intact, as the horizontal, vertical, and diagonal details are maintained by $\mathbb{H}$, $\mathbb{V}$, and $\mathbb{D}$ bands, respectively (Ali and Ahn, 2014).

The approximation band $\mathbb{A}$ is decomposed into distinct blocks $\mathbb{B}_i$, where $i \in [1, \frac{M\times N}{64}]$. Consequently, in total $\frac{M\times N}{64}$ unique blocks are created and each block has dimension 4×4.

A set of unique numbers is defined to satisfy the condition, $k = \{1, 2, \ldots, \lceil \frac{M\times N}{64} \rceil\}$. The blocks selected based on k are decomposed using SVD into right $\boldsymbol{U}$, left $\boldsymbol{V}$ vectors, and singular values λ:

$$\mathbb{B}_i = \boldsymbol{U}_i \lambda_i \boldsymbol{V}_i^{\mathrm{T}}, i = k = 1, 2, \ldots, \lceil \frac{M \times N}{64} \rceil. \quad (18)$$

Remark 3 A little disturbance in an image does not cause significant changes in the singular values, and vice versa (Santhi and Thangavelu, 2009; Bhagyashri and Joshi, 2011; Dharwadkar et al., 2011; Makbool and Khoo, 2014).

Remark 4 Singular values contain luminance information; in contrast, singular vectors possess geometric information (Bhagyashri and Joshi, 2011; Dharwadkar et al., 2011; Lai, 2011b; Makbool and Khoo, 2014).

The correlation matrix $\boldsymbol{C}$ for each block $\mathbb{B}_i$ is computed. Based on the correlation matrix, among the four columns, the column least dependent on another is selected. We define the least dependent column s. Similarly, from that column s, the two least correlated values are found, whose locations are defined as y and z. Then the two elements located at (y, s) and (z, s) in $\boldsymbol{U}_i$, two elements located at (s, y) and (s, z) in $\boldsymbol{V}_i$, and one singular value either (y, y) if $y > z$ or (z, z) if $y < z$ in λ_i, are selected for modification. The embedding process is discussed in detail below:

(1) Watermarking bit is 1 and $y < z$:

$$\begin{cases} U_{\mathrm{w}i}(y,s)=\mathrm{sgn}\big(U_i(y,s)\big)\cdot\Big(\tilde{U}_i+\gamma/2\Big), \\ U_{\mathrm{w}i}(z,s)=\mathrm{sgn}\big(U_i(z,s)\big)\cdot\Big(\tilde{U}_i-\gamma/2\Big), \\ V_{\mathrm{w}i}(s,y)=\mathrm{sgn}\big(V_i(s,y)\big)\cdot\Big(\tilde{V}_i+\gamma/2\Big), \\ V_{\mathrm{w}i}(s,z)=\mathrm{sgn}\big(V_i(s,z)\big)\cdot\Big(\tilde{V}_i-\gamma/2\Big), \\ \lambda_{\mathrm{w}i}(z,z)=2\lambda_i(y,y). \end{cases} \quad (19)$$

(2) Watermarking bit is 1 and $y > z$:

$$\begin{cases} U_{\mathrm{w}i}(z,s)=\mathrm{sgn}\big(U_i(z,s)\big)\cdot\Big(\tilde{U}_i+\gamma/2\Big), \\ U_{\mathrm{w}i}(y,s)=\mathrm{sgn}\big(U_i(y,s)\big)\cdot\Big(\tilde{U}_i-\gamma/2\Big), \\ V_{\mathrm{w}i}(s,z)=\mathrm{sgn}\big(V_i(s,z)\big)\cdot\Big(\tilde{V}_i+\gamma/2\Big), \\ V_{\mathrm{w}i}(s,y)=\mathrm{sgn}\big(V_i(s,y)\big)\cdot\Big(\tilde{V}_i-\gamma/2\Big), \\ \lambda_{\mathrm{w}i}(y,y)=2\lambda_i(z,z). \end{cases} \quad (20)$$

(3) Watermarking bit is 0 and $y < z$:

$$\begin{cases} U_{\mathrm{w}i}(y,s)=\mathrm{sgn}\big(U_i(y,s)\big)\cdot\Big(\tilde{U}_i-\gamma/2\Big), \\ U_{\mathrm{w}i}(z,s)=\mathrm{sgn}\big(U_i(z,s)\big)\cdot\Big(\tilde{U}_i+\gamma/2\Big), \\ V_{\mathrm{w}i}(s,y)=\mathrm{sgn}\big(V_i(s,y)\big)\cdot\Big(\tilde{V}_i-\gamma/2\Big), \\ V_{\mathrm{w}i}(s,z)=\mathrm{sgn}\big(V_i(s,z)\big)\cdot\Big(\tilde{V}_i+\gamma/2\Big), \\ \lambda_{\mathrm{w}i}(z,z)=2\lambda_i(y,y). \end{cases} \quad (21)$$

(4) Watermarking bit is 0 and $y > z$:

$$\begin{cases} U_{\mathrm{w}i}(z,s)=\mathrm{sgn}\big(U_i(z,s)\big)\cdot\Big(\tilde{U}_i-\gamma/2\Big), \\ U_{\mathrm{w}i}(y,s)=\mathrm{sgn}\big(U_i(y,s)\big)\cdot\Big(\tilde{U}_i+\gamma/2\Big), \\ V_{\mathrm{w}i}(s,z)=\mathrm{sgn}\big(V_i(s,z)\big)\cdot\Big(\tilde{V}_i-\gamma/2\Big), \\ V_{\mathrm{w}i}(s,y)=\mathrm{sgn}\big(V_i(s,y)\big)\cdot\Big(\tilde{V}_i+\gamma/2\Big), \\ \lambda_{\mathrm{w}i}(y,y)=2\lambda_i(z,z). \end{cases} \quad (22)$$

In Eqs. (19)–(22), $\tilde{U}_i = \frac{1}{2}|U_i(y,s) + U_i(z,s)|$, $\tilde{V}_i = \frac{1}{2}|V_i(s,y) + V_i(s,z)|$. The locations of the values and their corresponding columns are saved and are required later when the watermark is to be extracted. As a consequence, keys $\boldsymbol{Z}_q$ will be generated, $q = 1, 2, \ldots, \lceil \frac{M\times N}{64} \rceil$. Each key contains three numbers and represents the location of least correlated elements from a least correlated column.

Remark 5 Adding information into $\boldsymbol{U}$ results in a negligible change to the original image, whereas the addition of the same amount of information into the rows of $\boldsymbol{U}$ degrades the image quality severely. The opposite is true for $\boldsymbol{V}$(see the appendix).

The modified singular vectors $\boldsymbol{U}_{\mathrm{w}i}$ and $\boldsymbol{V}_{\mathrm{w}i}$ along with singular values $\lambda_{\mathrm{w}i}$ are used to obtain the watermark added blocks:

$$\mathbb{B}_{\mathrm{w}i} = \boldsymbol{U}_{\mathrm{w}i} \lambda_{\mathrm{w}i} \boldsymbol{V}_{\mathrm{w}i}^{\mathrm{T}}, \quad (23)$$

where $i = k = 1, 2, \ldots, \lceil \frac{M\times N}{64} \rceil$.

The watermark added blocks $\mathbb{B}_{\mathrm{w}i}$'s are properly combined to obtain the watermark added approximation band $\mathbb{A}_{\mathrm{w}}$.

The modified wavelet band along with unmodified bands is used to obtain the watermark added principal component:

$$\begin{aligned}\boldsymbol{P}_{\mathrm{w}}&=\begin{bmatrix}\boldsymbol{P}_{\boldsymbol{\rho}_{\mathrm{w}}} & \boldsymbol{P}_{\boldsymbol{\gamma}} & \boldsymbol{P}_{\boldsymbol{\beta}}\end{bmatrix}^{\mathrm{T}}\\&=\begin{bmatrix}\boldsymbol{P}_{\boldsymbol{\rho}_{\mathrm{w}1}} & \boldsymbol{P}_{\boldsymbol{\rho}_{\mathrm{w}2}} & \cdots & \boldsymbol{P}_{\boldsymbol{\rho}_{\mathrm{w}i}} & \cdots & \boldsymbol{P}_{\boldsymbol{\rho}_{\mathrm{w}M}}\\ \boldsymbol{P}_{\boldsymbol{\gamma}_1} & \boldsymbol{P}_{\boldsymbol{\gamma}_2} & \cdots & \boldsymbol{P}_{\boldsymbol{\gamma}_i} & \cdots & \boldsymbol{P}_{\boldsymbol{\gamma}_M}\\ \boldsymbol{P}_{\boldsymbol{\beta}_1} & \boldsymbol{P}_{\boldsymbol{\beta}_2} & \cdots & \boldsymbol{P}_{\boldsymbol{\beta}_i} & \cdots & \boldsymbol{P}_{\boldsymbol{\beta}_M}\end{bmatrix},\end{aligned}\tag{24}$$

where $\boldsymbol{P}_{\boldsymbol{\rho}_{\mathrm{w}i}}=[p_{\rho_{\mathrm{w}i1}},p_{\rho_{\mathrm{w}i2}},\ldots,p_{\rho_{\mathrm{w}iN}}]$.

$$\begin{aligned}&\begin{bmatrix}p_{\rho_{\mathrm{w}11}} & p_{\rho_{\mathrm{w}12}} & \cdots & p_{\rho_{\mathrm{w}1N}}\\ p_{\rho_{\mathrm{w}21}} & p_{\rho_{\mathrm{w}22}} & \cdots & p_{\rho_{\mathrm{w}2N}}\\ \vdots & \vdots & & \vdots\\ p_{\rho_{\mathrm{w}M1}} & p_{\rho_{\mathrm{w}M2}} & \cdots & p_{\rho_{\mathrm{w}MN}}\end{bmatrix}\\&=\mathrm{IDWT}(\mathbb{A}_{\mathrm{w}},\mathbb{H},\mathbb{V},\mathbb{D}).\end{aligned}\tag{25}$$

The principal components are used to obtain matrix $\boldsymbol{A}_{\mathrm{w}}$:

$$\begin{aligned}\boldsymbol{A}_{\mathrm{w}}&=\boldsymbol{\Phi}\boldsymbol{P}_{\mathrm{w}}\\&=\begin{bmatrix}\boldsymbol{\rho}_{\mathrm{w}1} & \boldsymbol{\rho}_{\mathrm{w}2} & \cdots & \boldsymbol{\rho}_{\mathrm{w}i} & \cdots & \boldsymbol{\rho}_{\mathrm{w}M}\\ \boldsymbol{\gamma}_1 & \boldsymbol{\gamma}_2 & \cdots & \boldsymbol{\gamma}_i & \cdots & \boldsymbol{\gamma}_M\\ \boldsymbol{\beta}_1 & \boldsymbol{\beta}_2 & \cdots & \boldsymbol{\beta}_i & \cdots & \boldsymbol{\beta}_M\end{bmatrix},\end{aligned}\tag{26}$$

where $\boldsymbol{\rho}_{\mathrm{w}i}=[\rho_{\mathrm{w}i1},\rho_{\mathrm{w}i2},\ldots,\rho_{\mathrm{w}iN}]$.

Finally, the watermarked-image $\boldsymbol{I}_{\mathrm{w}}$ is obtained using $\boldsymbol{I}_{\mathrm{R_w}}$, $\boldsymbol{I}_{\mathrm{G}}$, and $\boldsymbol{I}_{\mathrm{B}}$, where

$$\boldsymbol{I}_{\mathrm{R_w}}=\begin{bmatrix}\rho_{\mathrm{w}11} & \rho_{\mathrm{w}12} & \cdots & \rho_{\mathrm{w}1N}\\ \rho_{\mathrm{w}21} & \rho_{\mathrm{w}22} & \cdots & \rho_{\mathrm{w}2N}\\ \vdots & \vdots & & \vdots\\ \rho_{\mathrm{w}M1} & \rho_{\mathrm{w}M2} & \cdots & \rho_{\mathrm{w}MN}\end{bmatrix}.\tag{27}$$

2.2 Watermark extraction procedure

The received watermarked image $\hat{\boldsymbol{I}}_{\mathrm{w}}$ may have been subjected to some kind of degradation, due to intentional or unintentional attack. This image $\hat{\boldsymbol{I}}_{\mathrm{w}}$ is divided into its constituents:

$$\begin{aligned}\boldsymbol{I}_{\mathrm{Rw}}&=\begin{bmatrix}\hat{\rho}_{\mathrm{w}11} & \hat{\rho}_{\mathrm{w}12} & \cdots & \hat{\rho}_{\mathrm{w}1N}\\ \hat{\rho}_{\mathrm{w}21} & \hat{\rho}_{\mathrm{w}22} & \cdots & \hat{\rho}_{\mathrm{w}2N}\\ \vdots & \vdots & & \vdots\\ \hat{\rho}_{\mathrm{w}M1} & \hat{\rho}_{\mathrm{w}M2} & \cdots & \hat{\rho}_{\mathrm{w}MN}\end{bmatrix},\boldsymbol{I}_{\mathrm{G}}=\begin{bmatrix}\hat{\gamma}_{11} & \hat{\gamma}_{12} & \cdots & \hat{\gamma}_{1N}\\ \hat{\gamma}_{21} & \hat{\gamma}_{22} & \cdots & \hat{\gamma}_{2N}\\ \vdots & \vdots & & \vdots\\ \hat{\gamma}_{M1} & \hat{\gamma}_{M2} & \cdots & \hat{\gamma}_{MN}\end{bmatrix},\\ \boldsymbol{I}_{\mathrm{B}}&=\begin{bmatrix}\hat{\beta}_{11} & \hat{\beta}_{12} & \cdots & \hat{\beta}_{1N}\\ \hat{\beta}_{21} & \hat{\beta}_{22} & \cdots & \hat{\beta}_{2N}\\ \vdots & \vdots & & \vdots\\ \hat{\beta}_{M1} & \hat{\beta}_{M2} & \cdots & \hat{\beta}_{MN}\end{bmatrix}.\end{aligned}\tag{28}$$

The channels $\hat{\boldsymbol{I}}_{\mathrm{R_w}}$, $\hat{\boldsymbol{I}}_{\mathrm{G}}$, and $\hat{\boldsymbol{I}}_{\mathrm{B}}$ are used to obtain the correlation matrix $\hat{\boldsymbol{C}}$:

$$\begin{cases}\hat{\boldsymbol{C}}=\dfrac{1}{M\times N}\hat{\boldsymbol{A}}\hat{\boldsymbol{A}}^{\mathrm{T}}=\hat{\boldsymbol{\Phi}}\hat{\wedge}\hat{\boldsymbol{\Phi}}^{-1},\\ \hat{\boldsymbol{A}}=\begin{bmatrix}\hat{\boldsymbol{\rho}}_{\mathrm{w}1} & \hat{\boldsymbol{\rho}}_{\mathrm{w}2} & \cdots & \hat{\boldsymbol{\rho}}_{\mathrm{w}i} & \cdots & \hat{\boldsymbol{\rho}}_{\mathrm{w}M}\\ \hat{\boldsymbol{\gamma}}_1 & \hat{\boldsymbol{\gamma}}_2 & \cdots & \hat{\boldsymbol{\gamma}}_i & \cdots & \hat{\boldsymbol{\gamma}}_M\\ \hat{\boldsymbol{\beta}}_1 & \hat{\boldsymbol{\beta}}_2 & \cdots & \hat{\boldsymbol{\beta}}_i & \cdots & \hat{\boldsymbol{\beta}}_M\end{bmatrix},\\ \hat{\boldsymbol{\Phi}}=\begin{bmatrix}\hat{\phi}_{11} & \hat{\phi}_{12} & \hat{\phi}_{13}\\ \hat{\phi}_{21} & \hat{\phi}_{22} & \hat{\phi}_{23}\\ \hat{\phi}_{31} & \hat{\phi}_{32} & \hat{\phi}_{33}\end{bmatrix},\\ \hat{\wedge}=\begin{bmatrix}\hat{\wedge}_{11} & 0 & 0\\ 0 & \hat{\wedge}_{22} & 0\\ 0 & 0 & \hat{\wedge}_{33}\end{bmatrix},\end{cases}\tag{29}$$

where $\hat{\boldsymbol{\rho}}_{\mathrm{w}i}=[\hat{\rho}_{\mathrm{w}i1},\hat{\rho}_{\mathrm{w}i2},\ldots,\hat{\rho}_{\mathrm{w}iN}]$, $\hat{\boldsymbol{\gamma}}_i=[\hat{\gamma}_{i1},\hat{\gamma}_{i2},\ldots,\hat{\gamma}_{iN}]$, and $\hat{\boldsymbol{\beta}}_i=[\hat{\beta}_{i1},\hat{\beta}_{i2},\ldots,\hat{\beta}_{iN}]$.

The correlation matrix $\hat{\boldsymbol{C}}$ is used to obtain principal components:

$$\begin{aligned}\hat{\boldsymbol{P}}_{\mathrm{w}}&=\begin{bmatrix}\hat{\boldsymbol{P}}_{\boldsymbol{\rho}_{\mathrm{w}}} & \hat{\boldsymbol{P}}_{\boldsymbol{\gamma}} & \hat{\boldsymbol{P}}_{\boldsymbol{\beta}}\end{bmatrix}^{\mathrm{T}}\\&=\begin{bmatrix}\hat{\boldsymbol{P}}_{\boldsymbol{\rho}_{\mathrm{w}1}} & \hat{\boldsymbol{P}}_{\boldsymbol{\rho}_{\mathrm{w}2}} & \cdots & \hat{\boldsymbol{P}}_{\boldsymbol{\rho}_{\mathrm{w}i}} & \cdots & \hat{\boldsymbol{P}}_{\boldsymbol{\rho}_{\mathrm{w}M}}\\ \hat{\boldsymbol{P}}_{\boldsymbol{\gamma}_1} & \hat{\boldsymbol{P}}_{\boldsymbol{\gamma}_2} & \cdots & \hat{\boldsymbol{P}}_{\boldsymbol{\gamma}_i} & \cdots & \hat{\boldsymbol{P}}_{\boldsymbol{\gamma}_M}\\ \hat{\boldsymbol{P}}_{\boldsymbol{\beta}_1} & \hat{\boldsymbol{P}}_{\boldsymbol{\beta}_2} & \cdots & \hat{\boldsymbol{P}}_{\boldsymbol{\beta}_i} & \cdots & \hat{\boldsymbol{P}}_{\boldsymbol{\beta}_M}\end{bmatrix},\end{aligned}\tag{30}$$

where $\hat{\boldsymbol{P}}_{\boldsymbol{\rho}_{\mathrm{w}i}}=[\hat{p}_{\rho_{\mathrm{w}i1}},\hat{p}_{\rho_{\mathrm{w}i2}},\ldots,\hat{p}_{\rho_{\mathrm{w}iN}}]$, $\hat{\boldsymbol{P}}_{\boldsymbol{\gamma}_i}=[\hat{p}_{\gamma_{i1}},\hat{p}_{\gamma_{i2}},\ldots,\hat{p}_{\gamma_{iN}}]$, and $\hat{\boldsymbol{P}}_{\boldsymbol{\beta}_i}=[\hat{p}_{\beta_{i1}},\hat{p}_{\beta_{i2}},\ldots,\hat{p}_{\beta_{iN}}]$.

The matrix $\hat{\boldsymbol{P}}_{\boldsymbol{\rho}_{\mathrm{w}\,\mathrm{n}}}$ obtained from the 1st row of $\hat{\boldsymbol{P}}_{\mathrm{w}}$ is divided using DWT:

$$\begin{aligned}&(\hat{\mathbb{A}}_{\mathrm{w}},\hat{\mathbb{H}},\hat{\mathbb{V}},\hat{\mathbb{D}})=\mathrm{DWT}(\hat{\boldsymbol{P}}_{\boldsymbol{\rho}_{\mathrm{w}\,\mathrm{n}}}),\\&\hat{\boldsymbol{P}}_{\boldsymbol{\rho}_{\mathrm{w}\,\mathrm{n}}}=\begin{bmatrix}\hat{p}_{\rho_{\mathrm{w}11}} & \hat{p}_{\rho_{\mathrm{w}12}} & \cdots & \hat{p}_{\rho_{\mathrm{w}1N}}\\ \hat{p}_{\rho_{\mathrm{w}21}} & \hat{p}_{\rho_{\mathrm{w}22}} & \cdots & \hat{p}_{\rho_{\mathrm{w}2N}}\\ \vdots & \vdots & & \vdots\\ \hat{p}_{\rho_{\mathrm{w}M1}} & \hat{p}_{\rho_{\mathrm{w}M2}} & \cdots & \hat{p}_{\rho_{\mathrm{w}MN}}\end{bmatrix}.\end{aligned}\tag{31}$$

The received watermark added approximation band $\hat{\mathbb{A}}_{\mathrm{w}}$ is decomposed into distinct blocks $\hat{\mathbb{B}}_i$, $i\in[1,\frac{M\times N}{64}]$. Consequently, totally $\frac{M\times N}{64}$ unique blocks are created, and each block has dimension 4×4.

The blocks selected based on k are decomposed using SVD into right $\boldsymbol{U}$ and left $\boldsymbol{V}$ vectors and singular values λ:

$$\hat{\mathbb{B}}_i=\hat{\boldsymbol{U}}_i\hat{\lambda}_i\hat{\boldsymbol{V}}_i^{\mathrm{T}},\tag{32}$$

where $i=k=1,2,\ldots,\lceil\frac{M\times N}{64}\rceil$.

The keys $\boldsymbol{Z}_q$, $q=1,2,\ldots,\lceil\frac{M\times N}{64}\rceil$, are used here

to extract the hidden information (watermark):

$$\begin{cases} \hat{W}_i = \begin{cases} \Phi, & \text{if } (X=\Phi)\wedge(\Omega=\Phi), \\ \Psi, & \text{otherwise}, \end{cases} \\ X = \begin{cases} 1, \hat{U}_{\mathrm{w}_i}(Z_q(2),Z_q(1)) \le \hat{U}_{\mathrm{w}_i}(Z_q(3),Z_q(1)), \\ 0, \text{otherwise}, \end{cases} \\ \Omega = \begin{cases} 1, \hat{V}_{\mathrm{w}_i}(Z_q(1),Z_q(2)) \le \hat{V}_{\mathrm{w}_i}(Z_q(1),Z_q(3)), \\ 0, \text{otherwise}, \end{cases} \\ \Phi = \begin{cases} 1, \hat{\lambda}_{\mathrm{w}_i}(Z_q(2),Z_q(2)) \le \hat{\lambda}_{\mathrm{w}_i}(Z_q(3),Z_q(3)), \\ 0, \text{otherwise}, \end{cases} \\ \Psi = \mathrm{mode}\{X,\Omega,\Phi\}. \end{cases} \tag{33}$$

3 Experimental results

To evaluate the proposed technique, several experiments were conducted. Six diverse images (Fig. 6) were chosen as host images. These images vary in their appearance: some of them are smooth while others are highly textured. This was done intentionally to evaluate the performance of the technique for different images and obtain satisfactory results. Similarly, two binary images (Fig. 7a is a simple logo and Fig. 7b is a binary pattern) are used as watermarks. The evaluation of the scheme is discussed in detail in subsequent subsections.

3.1 Imperceptibility

The first challenge a watermarking scheme must confront is to obtain visually almost the same image after watermark embedding as it was before. This is defined as imperceptibility (Mohanty et al., 2006). To measure imperceptibility quantitatively, a metric called the peak signal-to-noise ratio (PSNR) is used (Mohanty et al., 2006; Makbool and Khoo, 2014). The formula to calculate PSNR (Drew and Bergner, 2008; Chen et al., 2014) is shown in Eq. (34):

$$\begin{cases} \mathrm{PNSR}_{\mathrm{dB}} = 10\lg\dfrac{255^2}{\mathrm{MSE}}, \\ \mathrm{MSE} = \dfrac{1}{3MN}\displaystyle\sum_{x=0}^{M-1}\sum_{y=0}^{N-1}\sum_{k}(I_k(x,y)-I_{k\mathrm{w}}(x,y)), \end{cases} \tag{34}$$

where $\boldsymbol{I}_k$ denotes the original image, $\boldsymbol{I}_{k\mathrm{w}}$ represents the watermarked image, and $k \in \{\mathrm{R},\mathrm{G},\mathrm{B}\}$.

The PSNR values of the scheme for all images (Gonzalez and Woods, 2008) are shown in Table 1 for a wide range of scaling factors.

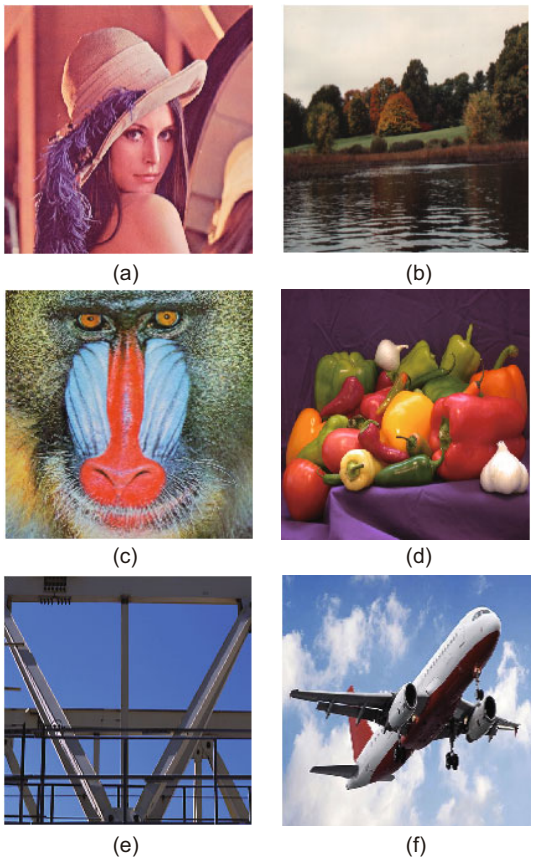

Fig. 6 Host images (512×512): (a) Lena; (b) Baboon; (c) Scenery; (d) Plane; (e) Peppers; (f) Crane

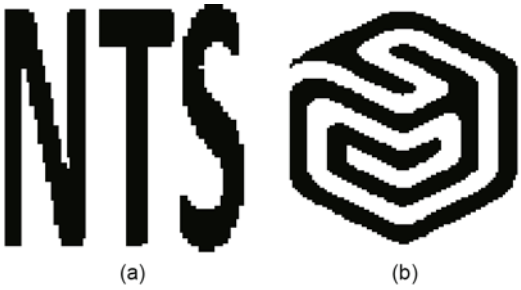

Fig. 7 Original watermark: (a) simple logo; (b) binary pattern

Table 1 PSNR values of different images for a range of scaling factors

Image	PSNR (dB)				
	$\gamma=0.01$	$\gamma=0.03$	$\gamma=0.05$	$\gamma=0.07$	$\gamma=0.09$
Lena	57.1587	55.9607	54.7786	53.6421	52.6026
Baboon	46.6570	46.1122	45.5749	45.0376	44.5172
Scenery	55.3104	52.4579	50.0438	47.9565	46.2196
Plane	54.8142	53.7218	52.6163	51.5416	50.5498
Peppers	59.0879	57.0622	55.1202	53.4783	52.0509
Crane	54.4168	53.5423	52.6743	51.8306	51.0145

At the same time, the comparison of the proposed scheme with the latest techniques is shown in

Table 2, with $\gamma = 0.05$ and the watermark shown in Fig. 7b. It is evident from Table 2 that the proposed technique is better than the existing techniques (Roy et al., 2015; Fazli and Moeini, 2016) in terms of PSNR.

Table 2 PSNR values of the proposed scheme and existing schemes for comparison

Image	PSNR (dB)		
	Proposed	Fazli and Moeini (2016)	Roy et al. (2015)
Lena	54.7786	38.1630	33.6223
Baboon	45.5749	32.5976	26.9310
Scenery	50.0438	34.7439	32.4283
Plane	52.6163	36.4416	33.9467
Pepper	55.1202	37.3452	32.0110
Crane	52.1202	38.9102	35.9553

Another way to measure imperceptibility is by qualitative analysis. To do so, both original and watermarked images are presented to the end user. The watermark images are shown in Fig. 8. It is clearly seen that for a human eye, there is no perceptible difference between the original (Fig. 6) and the watermarked images (Fig. 8). This further strengthens the evidence that the proposed scheme's performance is satisfactory in terms of imperceptibility.

In addition to the above images (Fig. 6), we compared 21 different images from the Kodak image database (Kodak, 2013) to investigate the performance of the proposed scheme. The comparison of the proposed technique with the state-of-the-art techniques (Han et al., 2017; Vo et al., 2017), in terms of PSNR, is shown in Fig. 9. It is evident that the proposed scheme outperforms the existing techniques in terms of imperceptibility.

Another metric called the structural similarity index (SSIM) (Roy et al., 2015), shown in Eq. (35), is used to evaluate the quality of watermarked images with respect to the original host images:

$$\mathrm{SSIM} = \frac{(2\mu_{\boldsymbol{I}}\mu_{\boldsymbol{I}_\mathrm{w}} + K_1)(2\rho_{\boldsymbol{I}}\rho_{\boldsymbol{I}_\mathrm{w}} + K_2)}{(2\mu_{\boldsymbol{I}}^2\mu_{\boldsymbol{I}_\mathrm{w}}^2 + K_1)(2\rho_{\boldsymbol{I}}^2\rho_{\boldsymbol{I}_\mathrm{w}}^2 + K_2)}, \quad (35)$$

where $\mu_{\boldsymbol{I}}$ and $\mu_{\boldsymbol{I}_\mathrm{w}}$ denote the means of the original and watermarked images respectively, and $\rho_{\boldsymbol{I}}$ and $\rho_{\boldsymbol{I}_\mathrm{w}}$ represent the variances of the original and watermarked images respectively. K_1 and K_2 are constants almost equal to zero, used to avoid the circumstance in which the summation of means or variances becomes zero. The comparison in terms of

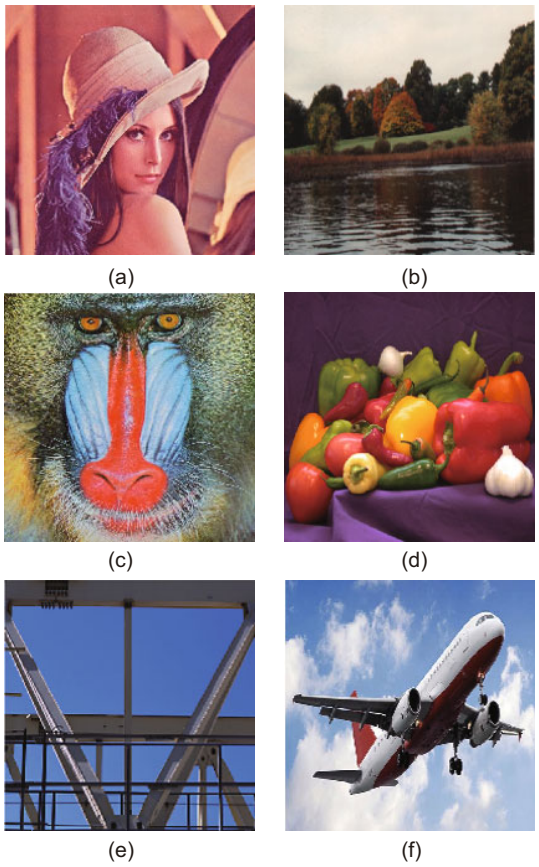

Fig. 8 Watermarked images (512×512): (a) Lena; (b) Baboon; (c) Scenery; (d) Plane; (e) Peppers; (f) Crane

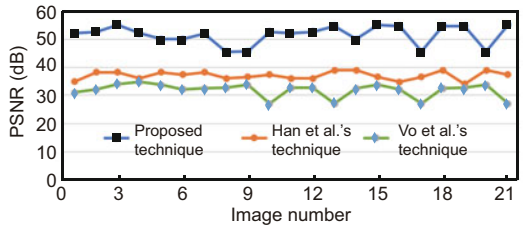

Fig. 9 Comparison of the proposed techique with other techiques (Han et al., 2017; Vo et al., 2017) in terms of PSNR using the Kodak database

SSIM with $\gamma = 0.05$ of the proposed technique with the existing techniques (Roy et al., 2015; Fazli and Moeini, 2016) is shown in Fig. 10. It is clearly seen that the quality of watermarked images obtained using the proposed technique is much better than that of the latest watermarking schemes.

3.2 Robustness

The watermarked image, once obtained successfully with good PSNR, may then be subjected to degradation due to attack. These attacks may be

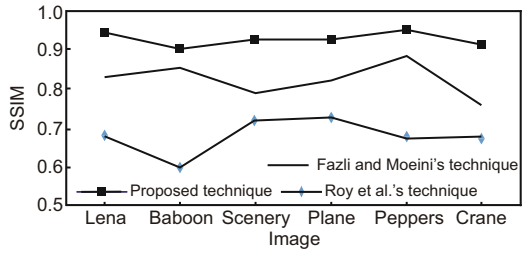

Fig. 10 Comparison of the proposed techique with other techiques (Roy et al., 2015; Fazli and Moeini, 2016) in terms of SSIM

intentional to destroy (remove) the watermark or unintentional. Whatever the case, it is difficult to extract a recognizable watermark from attacked or degraded watermarked images. This leads us to a second requisite: in spite of being attacked on watermarked images, the watermarking scheme must be robust enough to extract the recognizable watermark (Makbool and Khoo, 2014).

We have designed several attacks to evaluate the performance pertinent to robustness, such as histogram equalization (HIEQ), speckle noise (SKLNO), X-shearing (XSHER), JPEG compression (COMP), average filtering (AVGFL), salt & pepper noise (S&PNO), translation (TRLA), Gaussian noise (GAUNO), Y-shearing (YSHER), motion blurring (MOTBL), scaling (SCAL), affine transformation (AFTRA), rotation (ROTN), simple blurring (SIMBL), and cropping (CROP). These attacks with different parameters, as shown in Table 3, were applied on watermarked images. Then watermarks were retrieved from those distorted watermarked images.

Like imperceptibility, robustness can also be

Table 3 Normalized correlation (NC) for different attacks

Attack	Parameter	NC				
		$\gamma = 0.01$	$\gamma = 0.03$	$\gamma = 0.05$	$\gamma = 0.07$	$\gamma = 0.09$
ROTN	$\phi = 45°$	0.7367	0.8313	0.8281	0.8320	0.8329
	$\phi = 90°$	0.8134	0.8288	0.8304	0.8325	0.8308
	$\phi = 135°$	0.7434	0.8188	0.8192	0.8206	0.8232
TRLA	Displaced by 40%	0.8608	0.8570	0.8572	0.8608	0.8581
	Displaced by 60%	0.8190	0.8540	0.8545	0.8486	0.8529
	Displaced by 120%	0.7623	0.8368	0.8370	0.8409	0.8384
XSHER	Sheared by −0.5 factor	0.7984	0.8375	0.8391	0.8402	0.8430
	Sheared by −0.4 factor	0.8439	0.8430	0.8446	0.8459	0.8432
YSHER	Sheared by 0.5 factor	0.8434	0.8514	0.8473	0.8563	0.8505
	Sheared by 0.4 factor	0.8439	0.8437	0.8428	0.8384	0.8439
AFTRA	Sheared by 0.5 factor	0.7986	0.8197	0.8188	0.8148	0.8188
	Sheared by 0.4 factor	0.8227	0.8262	0.8285	0.8290	0.8213
SCAL	Scaled up 3×	0.9759	0.9828	0.9818	0.9816	0.9816
	Scaled up 0.5×	0.9462	0.9547	0.9551	0.9557	0.9583
CROP	Cropped 10% from center	0.8830	0.8845	0.8821	0.8817	0.8827
	Cropped 25% from sides	0.8563	0.8639	0.8648	0.8656	0.8645
GAUNO	$m = 0.0$, $\rho^2 = 0.01$	0.9019	0.9097	0.9025	0.9124	0.9156
	$m = 0.4$, $\rho^2 = 0.01$	0.8838	0.8897	0.8871	0.8903	0.8916
	$m = 0.5$, $\rho^2 = 0.5$	0.8751	0.8690	0.8729	0.8740	0.8790
S&PNO	10% density	0.8922	0.8920	0.8984	0.9027	0.8993
	50% density	0.8612	0.8554	0.8683	0.8665	0.8596
SKLNO	10% density	0.8927	0.8976	0.8974	0.8970	0.8974
	50% density	0.8623	0.8643	0.8594	0.8567	0.8603
Blurring	SIMBL	0.8920	0.8980	0.8995	0.8987	0.9016
	MOTBL	0.8881	0.8907	0.8922	0.8909	0.8890
AVGFL	3×3	0.9342	0.9424	0.9472	0.9477	0.9483
	5×5	0.9002	0.9008	0.9027	0.9052	0.9093
	7×7	0.8942	0.8957	0.8976	0.8980	0.8950
HIEQ		0.8616	0.8629	0.8636	0.8643	0.8656
COMP	Quality factor=30	0.8411	0.8383	0.7906	0.7853	0.7754
	Quality factor=50	0.8630	0.8612	0.8639	0.8610	0.8590
	Quality factor=70	0.8798	0.8955	0.9034	0.9299	0.9306

ROTN: rotation; TRLA: translation; XSHER: X-shearing; YSHER: Y-shearing; AFTRA: affine transformation; SCAL: scaling; CROP: cropping; GAUNO: Gaussian noise; S&PNO: salt & pepper noise; SKLNO: speckle noise; MOTBL: motion blurring; SIMBL: simple blurring; AVGFL: average filtering; HIEQ: histogram equalization; COMP: JPEG compression

measured quantitatively, using normalized correlation (NC) (Luo et al., 2010). NC values of the proposed scheme for retrieved watermarks are shown in Table 3. The scheme is compared with other existing schemes, as shown in Table 4. To achieve the results in Tables 3 and 4, the watermark shown in Fig. 7a was used.

$$\mathrm{NC}=\frac{\sum_{s=1}^{S}\sum_{t=1}^{T}\left(W(s,t)\widehat{W}(s,t)\right)}{\sqrt{\sum_{s=1}^{S}\sum_{t=1}^{T}W^2(s,t)}\sqrt{\sum_{s=1}^{S}\sum_{t=1}^{T}\widehat{W}^2(s,t)}}. \quad (36)$$

The proposed scheme also achieves better results than the latest watermarking techniques in terms of robustness. To further validate the performance of the scheme, the watermarks extracted for qualitative analysis are shown in Fig. 11. It can be seen that the watermarks extracted are identifiable and therefore are sufficient to claim ownership.

The bit error rate (BER) (Luo et al., 2010) is another way to measure the robustness of watermarking techniques (Ranjbara et al., 2013; Prathap et al., 2014). Comparison of the proposed techique with other techiques (Roy et al., 2015; Fazli and Moeini, 2016) in terms of BER is shown in Table 5.

$$\mathrm{BER}=\frac{\text{Number of wrong bits extracted}}{\text{Total number of bits embedded}}. \quad (37)$$

In addition to NC and BER, the normalized hamming distance (NHD) (Ranjbara et al., 2013) is used to authenticate the robustness:

$$\begin{cases}\mathrm{NHD}=\dfrac{1}{XY}\displaystyle\sum_{x=1}^{X}\sum_{y=1}^{Y}h_{w\hat{w}}(x,y),\\ h_{w\hat{w}}(x,y)=\begin{cases}1, & \text{if } w(x,y)=\hat{w}(x,y),\\ 0, & \text{otherwise.}\end{cases}\end{cases} \quad (38)$$

The comparison of the proposed scheme using NHD with other existing schemes (Table 6) shows a significant improvement over the state-of-the-art watermarking schemes (Roy et al., 2015; Fazli and Moeini, 2016).

3.3 Capacity

The watermarking scheme must be designed in such a way that it can conceal as much information as possible into the host image without compromising its visual quality, which is called capacity. The involvement of singular vectors ($\boldsymbol{U}$ and $\boldsymbol{V}$) and singular values (λ) significantly enhanced the capacity of the presented scheme. Therefore, for an image of size 512×512, the capacity is $3\times64\times64$, which is considered a high capacity. The capacity of the scheme proposed in Prathap et al. (2014) is 64×64. The capacity of the proposed scheme is twice more than the capacities of the schemes proposed in Roy et al. (2015) and Fazli and Moeini (2016).

Table 4 Normalized correlation (NC) for different techniques

Attack	NC for Lena			NC for Peppers		
	Proposed	Fazli and Moeini (2016)	Roy et al. (2015)	Proposed	Fazli and Moeini (2016)	Roy et al. (2015)
ROTN	0.7367	0.5617	0.4507	0.8329	0.7116	0.5281
TRLA	0.7623	0.5675	0.4857	0.8384	0.7965	0.5764
XSHER	0.7984	0.6255	0.5019	0.8430	0.7288	0.5419
YSHER	0.8439	0.6796	0.5559	0.8439	0.7392	0.6294
AFTRA	0.8227	0.7651	0.6010	0.8213	0.7671	0.5852
SCAL	0.9462	0.8508	0.7254	0.9583	0.8379	0.5868
CROP	0.8563	0.7298	0.5575	0.8645	0.7825	0.6214
GAUNO	0.8751	0.7980	0.6458	0.8790	0.7869	0.5911
S&PNO	0.8612	0.7342	0.6307	0.8596	0.7311	0.5369
SKLNO	0.8623	0.7338	0.6023	0.8603	0.7872	0.5524
MOTBL	0.8920	0.7979	0.7176	0.9016	0.7802	0.6094
SIMBL	0.8881	0.7451	0.6792	0.8890	0.7793	0.5638
AVGFL	0.9002	0.7558	0.6764	0.9093	0.6948	0.5725
HIEQ	0.8616	0.7451	0.6578	0.8656	0.7181	0.5595
COMP	0.8630	0.6871	0.6466	0.8590	0.7659	0.5603

ROTN: rotation; TRLA: translation; XSHER: X-shearing; YSHER: Y-shearing; AFTRA: affine transformation; SCAL: scaling; CROP: cropping; GAUNO: Gaussian noise; S&PNO: salt & pepper noise; SKLNO: speckle noise; MOTBL: motion blurring; SIMBL: simple blurring; AVGFL: average filtering; HIEQ: histogram equalization; COMP: JPEG compression

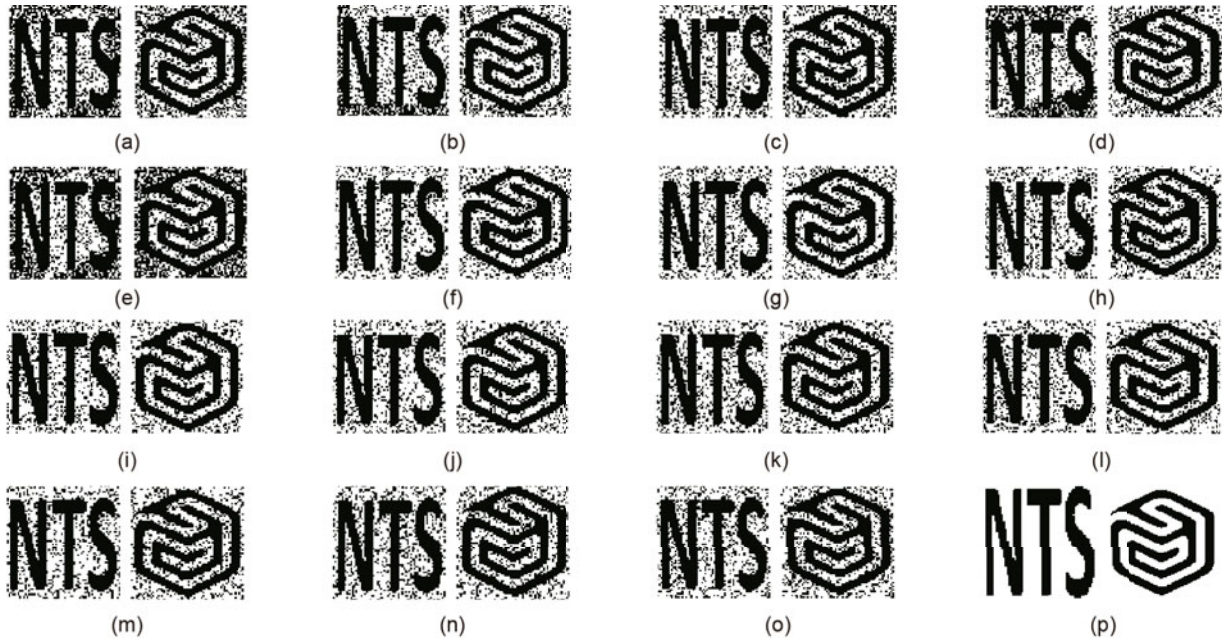

Fig. 11 Watermarks extracted from attacks: (a) ROTN; (b) TRLA; (c) XSHER; (d) YSHER; (e) AFTRA; (f) SCAL; (g) CROP; (h) GAUNO; (i) S&PNO; (j) SKLNO; (k) SIMBL; (l) MOTBL; (m) AVGFL; (n) HIEQ; (o) COMP; (p) original watermark

ROTN: rotation; TRLA: translation; XSHER: X-shearing; YSHER: Y-shearing; AFTRA: affine transformation; SCAL: scaling; CROP: cropping; GAUNO: Gaussian noise; S&PNO: salt & pepper noise; SKLNO: speckle noise; MOTBL: motion blurring; SIMBL: simple blurring; AVGFL: average filtering; HIEQ: histogram equalization; COMP: JPEG compression

Table 5 Bit error rate (BER) for different techniques

Attack	BER for Lena			BER for Baboon		
	Proposed	Fazli and Moeini (2016)	Roy et al. (2015)	Proposed	Fazli and Moeini (2016)	Roy et al. (2015)
ROTN	0.1963	0.2938	0.3532	0.2319	0.3470	0.4172
TRLA	0.1563	0.2189	0.2370	0.1592	0.2230	0.2414
XSHER	0.1829	0.2202	0.2684	0.1931	0.2325	0.2834
YSHER	0.2383	0.2641	0.2852	0.2395	0.2654	0.2866
AFTRA	0.2061	0.1827	0.2386	0.2825	0.2505	0.3270
SCAL	0.0520	0.0775	0.1138	0.0647	0.0964	0.1415
CROP	0.1406	0.2095	0.2485	0.1450	0.2161	0.2562
GAUNO	0.1106	0.1360	0.1844	0.0840	0.1033	0.1401
S&PNO	0.1179	0.1481	0.2022	0.1072	0.1346	0.1838
SKLNO	0.1255	0.1830	0.2425	0.1108	0.1615	0.2141
MOTBL	0.1191	0.1686	0.2232	0.1699	0.2406	0.3183
SIMBL	0.1338	0.2107	0.2788	0.1545	0.2433	0.3219
AVGFL	0.1104	0.1777	0.2370	0.1340	0.2156	0.2876
HIEQ	0.0413	0.0523	0.0700	0.0391	0.0496	0.0663
COMP	0.0847	0.1123	0.1371	0.0388	0.0515	0.0628

ROTN: rotation; TRLA: translation; XSHER: X-shearing; YSHER: Y-shearing; AFTRA: affine transformation; SCAL: scaling; CROP: cropping; GAUNO: Gaussian noise; S&PNO: salt & pepper noise; SKLNO: speckle noise; MOTBL: motion blurring; SIMBL: simple blurring; AVGFL: average filtering; HIEQ: histogram equalization; COMP: JPEG compression

3.4 Security

The fourth and also the last requisite a watermarking scheme must meet is security (Makbool and Khoo, 2014). A watermarking scheme is said to be secure if only the authorized personnel with the help of a genuine key can extract a watermark. To test the security of the proposed scheme, numerous fake

Table 6 Normalized Hamming distance (NHD) for different techniques

Attack	NHD for Baboon			NHD for Peppers		
	Proposed	Fazli and Moeini (2016)	Roy et al. (2015)	Proposed	Fazli and Moeini (2016)	Roy et al. (2015)
ROTN	0.7363	0.5614	0.4669	0.7334	0.5592	0.4650
TRLA	0.8213	0.6114	0.5647	0.8109	0.6037	0.5575
XSHER	0.8328	0.6525	0.5353	0.8042	0.6301	0.5169
YSHER	0.8391	0.6757	0.6258	0.8438	0.6795	0.6293
AFTRA	0.8052	0.7488	0.5737	0.7173	0.6671	0.5111
SCAL	0.9514	0.8555	0.5826	0.9592	0.8625	0.5873
CROP	0.8689	0.7405	0.6245	0.8606	0.7334	0.6186
GAUNO	0.8735	0.7965	0.5874	0.8801	0.8025	0.5918
S&PNO	0.8699	0.7416	0.5433	0.8728	0.7440	0.5451
SKLNO	0.8726	0.7425	0.5603	0.8745	0.7441	0.5615
MOTBL	0.8926	0.7984	0.6033	0.8933	0.7990	0.6038
SIMBL	0.8748	0.7340	0.5548	0.8833	0.7411	0.5602
AVGFL	0.9158	0.7689	0.5766	0.9207	0.7730	0.5797
HIEQ	0.9507	0.8221	0.6145	0.9375	0.8107	0.6060
COMP	0.9004	0.7169	0.5873	0.8833	0.7033	0.5762

ROTN: rotation; TRLA: translation; XSHER: X-shearing; YSHER: Y-shearing; AFTRA: affine transformation; SCAL: scaling; CROP: cropping; GAUNO: Gaussian noise; S&PNO: salt & pepper noise; SKLNO: speckle noise; MOTBL: motion blurring; SIMBL: simple blurring; AVGFL: average filtering; HIEQ: histogram equalization; COMP: JPEG compression

(false) keys were created and then with the help of those keys watermarks were extracted. Despite several attempts with several keys, no recognizable watermark was extracted. For simplicity, the watermarks extracted using 16 different fake keys are shown in Fig. 12. It is obvious that not a single retrieved watermark is recognizable, which illustrates the high security level of the proposed scheme.

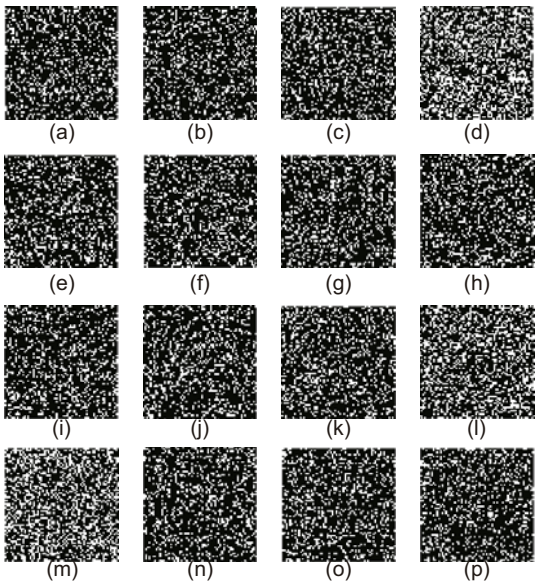

Fig. 12 Watermarks retrieved using incorrect security keys: (a) ROTN; (b) TRLA; (c) XSHER; (d) YSHER; (e) AFTRA; (f) SCAL; (g) CROP; (h) GAUNO; (i) S&PNO; (j) SKLNO; (k) SIMBL; (l) MOTBL; (m) AVGFL; (n) HIEQ; (o) COMP; (p) original watermark

ROTN: rotation; TRLA: translation; XSHER: X-shearing; YSHER: Y-shearing; AFTRA: affine transformation; SCAL: scaling; CROP: cropping; GAUNO: Gaussian noise; S&PNO: salt & pepper noise; SKLNO: speckle noise; MOTBL: motion blurring; SIMBL: simple blurring; AVGFL: average filtering; HIEQ: histogram equalization; COMP: JPEG compression

4 Conclusions

A block-based secure and robust watermarking technique is presented for color images based on multi-resolution decomposition and de-correlation. The main objective is to design a watermarking scheme that can meet almost all requirements of a watermarking scheme. To do so, the mutually dependent color channels are de-correlated, and after multiple resolution decompositions, a band is chosen in such a way that textural information does not get changed by embedding the watermark. Then, a novel approach is adopted to select the values for watermark embedding. The locations of values chosen for watermark embedding are used as secret keys. This novel approach can obtain good results in terms of robustness, imperceptibility, capacity, and security.

Compliance with ethics guidelines

Muhammad IMRAN, Bruce A. HARVEY, Muhammad ATIF, and Adnan Ali MEMON declare that they have no conflict of interest.

References

Ali M, Ahn WC, 2014. An optimized watermarking technique based on self-adaptive DE in DWT-SVD transform domain. *Signal Process*, 94:545-556. https://doi.org/10.1016/j.sigpro.2013.07.024

Amini M, Ahmad MO, Swamy MNS, 2017a. A new locally optimum watermark detection using vector-based hidden Markov model in wavelet domain. *Signal Process*, 137:213-222. https://doi.org/10.1016/j.sigpro.2017.01.019

Amini M, Sadreazami H, Ahmad MO, et al., 2017b. A hidden Markov model-based blind detector for multiplicative watermarking. 60th Int Midwest Symp on Circuits and Systems, p.176-179. https://doi.org/10.1109/MWSCAS.2017.8052997

Amini M, Sadreazami H, Ahmad MO, et al., 2017c. Multichannel color image watermark detection utilizing vector-based hidden Markov model. Int Symp on Circuits and Systems, p.1-4. https://doi.org/10.1109/ISCAS.2017.8050596

Barni M, Bartolini F, Piva A, 2001. Improved wavelet-based watermarking through pixel-wise masking. *IEEE Trans Image Process*, 10(5):783-791. https://doi.org/10.1109/83.918570

Bhagyashri SK, Joshi MY, 2011. All frequency band DWT-SVD robust watermarking technique for color images in YUV color space. IEEE Int Conf on Computer Science and Automation Engineering, p.295-299. https://doi.org/10.1109/CSAE.2011.5952684

Chang SC, Shen JJ, 2017. Features classification forest: a novel development that is adaptable to robust blind watermarking techniques. *IEEE Trans Image Process*, 26(8):3921-3935. https://doi.org/10.1109/TIP.2017.2706502

Chen B, Coatrieux G, Chen G, et al., 2014. Full 4-D quaternion discrete Fourier transform based watermarking for color images. *Dig Signal Process*, 28:106-119. https://doi.org/10.1016/J.DSP.2014.02.010

Chou HC, Liu CK, 2010. A perceptually tuned watermarking scheme for color images. *IEEE Trans Image Process*, 19(11):2966-2982. https://doi.org/10.1109/TIP.2010.2052261

Dharwadkar VN, Amberker BB, Gorai A, 2011. Non-blind watermarking scheme for color images in RGB space using DWT-SVD. Int Conf on Communications and Signal Processing, p.489-493. https://doi.org/10.1109/ICCSP.2011.5739368

Drew SM, Bergner S, 2008. Spatio-chromatic decorrelation for color image compression. *Signal Process Image Commun*, 23(8):599-609. https://doi.org/10.1016/J.IMAGE.2008.05.006

Fazli S, Moeini M, 2016. A robust image watermarking method based on DWT, DCT, and SVD using a new technique for correction of main geometric attacks. *Optik*, 127(2):964-972. https://doi.org/10.1016/J.IJLEO.2015.09.205

Gonzalez RC, Woods RE, 2008. Wavelet and multiresolution processing. In: Gonzalez RC, Woods RE (Eds.), Digital Image Processing. Prentice Hall, USA.

Gunjal BL, Mali NS, 2011. Comparative performance analysis of DWT-SVD based color image watermarking technique in YUV, RGB and YIQ color spaces. *Int J Comput Theory Eng*, 3(6):714-717. https://doi.org/10.7763/IJCTE.2011.V3.397

Han S, Yang J, Wang R, et al., 2017. A novel color image watermarking algorithm based on QWT and DCT. Chinese Conf on Computer Vision, p.428-438. https://doi.org/10.1007/978-981-10-7299-4_35

Hernandez MC, Miyatake MN, Meana HMP, 2005. Analysis of a DFT-based watermarking algorithm. 2nd Int Conf on Electrical and Electronics Engineering, p.44-47. http://doi.org/10.1109/ICEEE.2005.1529569

Kalantari NK, Ahadi SM, Vfadust M, 2010. A robust image watermarking in the ridgelet domain using universally optimum decoder. *IEEE Trans Circ Syst Video Technol*, 20(3):396-406. https://doi.org/10.1109/TCSVT.2009.2035842

Kodak, 2013. University of Sheffield Library. http://www.r0k.us/graphics/kodak [Accessed on Dec. 15, 2017].

Lai CC, 2011a. A digital watermarking scheme based on singular value decomposition and tiny genetic algorithm. *Dig Signal Process*, 21(4):522-527. https://doi.org/10.1016/J.DSP.2011.01.017

Lai CC, 2011b. An improved SVD-based watermarking scheme using human visual characteristics. *Opt Commun*, 284(4):938-944. https://doi.org/10.1016/J.OPTCOM.2010.10.047

Lai CC, Tsai CC, 2010. Digital image watermarking using discrete wavelet transform and singular value decomposition. *IEEE Trans Instrum Meas*, 59(11):3060-3063. https://doi.org/10.1109/TIM.2010.2066770

Lina SD, Shieb SC, Guoa JY, 2010. Improving the robustness of DCT-based image watermarking against JPEG compression. *Comput Stand Interf*, 32(1-2):54-60. https://doi.org/10.1016/J.CSI.2009.06.004

Liu R, Tan T, 2002. An SVD based watermarking scheme for protecting rightful ownership. *IEEE Trans Multim*, 4(1):121-128. https://doi.org/10.1109/6046.985560

Loukhaoukha K, 2013. Comments on "A digital watermarking scheme based on singular value decomposition and tiny genetic algorithm". *Dig Signal Process*, 23(4):1334. https://doi.org/10.1016/J.DSP.2013.02.006

Luo L, Chen Z, Chen M, et al., 2010. Reversible image watermarking using interpolation technique. *IEEE Trans Inform Forens Secur*, 5(1):187-193. https://doi.org/10.1109/TIFS.2009.2035975

Makbool NM, Khoo BE, 2014. A new robust and secure digital image watermarking scheme based on the integer wavelet transform and singular value decomposition. *Dig Signal Process*, 33:134-147. https://doi.org/10.1016/J.DSP.2014.06.012

Meylan L, Susstrunk S, 2006. High dynamic range image rendering with a retinex-based adaptive filter. *IEEE Trans Image Process*, 15(9):2820-2830. https://doi.org/10.1109/TIP.2006.877312

Mohanty SP, Ranganathan N, Balakrishnan K, 2006. A dual voltage-frequency VLSI chip for image watermarking in DCT domain. *IEEE Trans Circ Syst*, 53(5):394-398. https://doi.org/10.1109/TCSII.2006.870216

Mudrová M, Procházka A, 2005. Principal component analysis in image processing. MATLAB Technical Computing Conf, p.1-4.

Prathap I, Natarajan V, Anitha R, 2014. Hybrid robust watermarking for color images. *Comput Electr Eng*, 40(3):920-930. https://doi.org/10.1016/j.compeleceng.2014.01.006

Ranjbara S, Zargarib F, Ghanbaric M, 2013. A highly robust two-stage Countourlet-based digital image watermarking method. *Signal Process Image Commun*, 28(10):1526-1536. https://doi.org/10.1016/J.IMAGE.2013.07.002

Roy A, Maiti AK, Ghosh K, 2015. A perception based color image adaptive watermarking scheme in YCbCr space. Int Conf on Signal Processing and Integrated Networks, p.537-543. https://doi.org/10.1109/spin.2015.7095399

Rykaczewski R, 2007. Comments on "An SVD based watermarking scheme for protecting rightful ownership". *IEEE Trans Multim*, 9(2):421-423. https://doi.org/10.1109/TMM.2006.886297

Sadreazami H, Amini M, 2012. A robust spread spectrum based image watermarking in ridgelet domain. *AEU Int J Electron Commun*, 66(5):364-371. https://doi.org/10.1016/j.aeue.2011.09.001

Sadreazami H, Ahmad MO, Swamy MNS, 2015. A robust multiplicative watermark detector for color images in sparse domain. *IEEE Trans Circ Syst*, 62(12):1159-1163. https://doi.org/10.1109/TCSII.2015.2468995

Santhi V, Thangavelu A, 2009. DWT-SVD combined full band robust watermarking technique for color images in YUV color space. *Int J Comput Theory Eng*, 1(4):424-429. https://doi.org/10.7763/IJCTE.2009.V1.68

Su Q, Niu Y, Liu X, et al., 2013. A novel blind digital watermarking algorithm for embedding color image into color imag. *Optik*, 124(18):3254-3259. https://doi.org/10.1016/J.IJLEO.2012.10.005

Sun X, Bo S, 2011. A blind digital watermarking for color medical images based on PCA. Int Conf on Wireless Communications, Networking, and Information Security, p.421-427. https://doi.org/10.1109/WCINS.2010.5541812

Tarisha M, 2017. The Politics of Online Copyright Enforcement in the EU. Palgrave Macmillan, Cham, USA. https://doi.org/10.1007/978-3-319-50974-7

Vidal R, Ma Y, Sastry S, 2005. Generalized principal component analysis. *IEEE Trans Patt Anal Mech Intell*, 27(12):1945-1959. https://doi.org/10.1109/TPAMI.2005.244

Vo PH, Nguyen TS, Huynh VT, et al., 2017. A robust hybrid watermarking scheme based on DCT and SVD for copyright protection of stereo images. 4th NAFOSTED Conf on Information and Computer Science, p.331-335. https://doi.org/10.1109/NAFOSTED.2017.8108087

Yavuz E, Telatar Z, 2013. Comments on "A digital watermarking scheme based on singular value decomposition and tiny genetic algorithm". *Dig Signal Process*, 23(4):1335-1336. https://doi.org/10.1016/J.DSP.2013.02.009

You X, Du L, Cheung Y, et al., 2010. A blind watermarking scheme using new non-tensor product wavelet filter banks. *IEEE Trans Inform Forens Secur*, 19(12):3271-3284. https://doi.org/10.1109/TIP.2010.2055570

Zhang PX, Li K, 2005. Comments on "An SVD based watermarking scheme for protecting rightful ownership". *IEEE Trans Multim*, 5(2):593-594. https://doi.org/10.1109/TMM.2005.843357

Zong T, Xiang Y, Natgunanathan I, et al., 2015. Robust histogram shape-based method for image watermarking. *IEEE Trans Circ Syst Video Technol*, 25(5):717-729. https://doi.org/10.1109/TCSVT.2014.2363743

Appendix: mathematical background

Consider that an image $\boldsymbol{A}$ of size $M \times N$ is decomposed into left singular vectors $\boldsymbol{U}$, singular values $\boldsymbol{S}$, and right singular vectors $\boldsymbol{V}$:

$$\begin{cases} \boldsymbol{A} = \boldsymbol{U}\boldsymbol{S}\boldsymbol{V}^{\mathrm{T}}, \\ \boldsymbol{U} = [u_{xx}], \boldsymbol{S} = [\lambda_{xy}], \boldsymbol{V} = [v_{yy}], \end{cases} \tag{A1}$$

where $1 \le x \le M$, $1 \le y \le N$, $\lambda_{xy} = 0$ when $x \ne y$.

Finding 1 The changes introduced in the columns of $\boldsymbol{U}$ are less perceptible in the original image $\boldsymbol{A}$ compared to the same number of changes introduced in the rows of $\boldsymbol{U}$.

The element of $\boldsymbol{A}$, a_{pq}, can be reconstructed from $\boldsymbol{U}$, $\boldsymbol{S}$, and $\boldsymbol{V}$, using the following relationship:

$$a_{pq} = \sum_{x=1}^{M}\sum_{y=1}^{N} u_{px}\lambda_{xy}v_{yq}, \tag{A2}$$

where $1 \le p \le M$, $1 \le q \le N$.

Replacing the first column of $\boldsymbol{U}$ ($u_{p1} = 0$), we can reduce Eq. (A2) to Eq. (A3):

$$a_{pq} = \sum_{x=2}^{M}\sum_{y=1}^{N} u_{px}\lambda_{xy}v_{qy}, \tag{A3}$$

where $1 \le p \le M$, $1 \le q \le N$.

Likewise, if the first row of $\boldsymbol{U}$ is set to 0 ($u_{1x} = 0$), we can reduce Eq. (A2) to Eq. (A4):

$$\begin{cases} a_{1q} = 0, \\ a_{2q} = \sum_{x=1}^{M}\sum_{y=1}^{N} u_{px}\lambda_{xy}v_{qy}, \end{cases} \tag{A4}$$

where $2 \le p \le M$, $1 \le q \le N$.

From Eq. (A3), it is clear that the changes in the original image $\boldsymbol{A}$ are evenly distributed over the whole image as a result of modifying the columns of $\boldsymbol{U}$, and consequently the changes are not perceptible

by the human eye, whereas, Eq. (A4) suggests that modifying elements of rows of $\boldsymbol{U}$ causes an entire row of the original image $\boldsymbol{U}$ to become zero, which in turn is easily perceptible by a human. Therefore, it is advisable that to embed a watermark, columns instead of rows of $\boldsymbol{U}$ should be chosen. Similarly, rows instead of columns of $\boldsymbol{V}$ should be changed to conceal a watermark.

Finding 2 The imperceptibility of a watermarked image further increases when the elements either from columns of $\boldsymbol{U}$ or from rows of $\boldsymbol{V}$ (least correlated elements) are chosen for watermark embedding.

In Finding 1, it is seen that modifying elements of columns of $\boldsymbol{U}$ causes less distortion to the original image compared to changing elements of rows of $\boldsymbol{U}$. Now to prove Finding 2, the elements from columns of $\boldsymbol{U}$ are chosen for watermark embedding based on the following three options: (1) Two elements (2^{nd} and 3^{rd}) from the first column of $\boldsymbol{U}$ are selected for modification; (2) Two least-correlated elements from the least-correlated column of $\boldsymbol{U}$ are selected for modification; (3) Two least-correlated elements from the first column of $\boldsymbol{U}$ are selected for modification.

The PSNR of watermarked images obtained using the above-mentioned options is shown in Fig. A1. It can be seen that modifying the least-correlated elements of a least-correlated column results in higher PSNR. Therefore, in the proposed scheme, option (2) of Finding 2 is adopted.

Finding 3 The robustness of a watermarking scheme further increases if both left ($\boldsymbol{U}$) and right ($\boldsymbol{V}$) singular vectors are involved in the watermark embedding process.

In Findings 1 and 2, it is seen that involving least-correlated elements from columns of $\boldsymbol{U}$ or from rows of $\boldsymbol{V}$ improves the imperceptibility. It is also suggested that involving both $\boldsymbol{U}$ and $\boldsymbol{V}$ improves imperceptibility. To prove this point, we consider that an image of size 4×4 is decomposed using SVD:

$$\begin{cases} \boldsymbol{A}=\boldsymbol{U}\boldsymbol{S}\boldsymbol{V}^{\mathrm{T}}, \\ \boldsymbol{A}=\begin{bmatrix}70 & 48 & 27 & 134\\ 25 & 39 & 122 & 203\\ 57 & 255 & 16 & 111\\ 35 & 167 & 131 & 158\end{bmatrix}, \\ \boldsymbol{U}=\begin{bmatrix}-0.32 & -0.20 & 0.80 & 0.46\\ -0.47 & -0.67 & -0.03 & -0.58\\ -0.57 & 0.72 & 0.17 & -0.37\\ -0.60 & -0.04 & -0.58 & 0.56\end{bmatrix}, \\ \boldsymbol{S}=\begin{bmatrix}442 & 0 & 0 & 0\\ 0 & 185 & 0 & 0\\ 0 & 0 & 78 & 0\\ 0 & 0 & 0 & 20\end{bmatrix}, \\ \boldsymbol{V}=\begin{bmatrix}-0.20 & 0.04 & 0.58 & 0.79\\ -0.63 & 0.75 & -0.20 & -0.06\\ -0.34 & -0.44 & -0.70 & 0.44\\ -0.67 & -0.49 & 0.38 & -0.41\end{bmatrix}. \end{cases} \tag{A5}$$

Suppose that the embedding bit is 1 and a condition is set. For instance, the condition $u_{31}<u_{21}$ indicates that the embedding bit is 1; the condition $u_{31}>u_{21}$ suggests that the embedding bit is 0. Keeping these conditions in view, the values of columns of $\boldsymbol{U}$ are modified as follows (for an embedding bit 0 and $\gamma=0.01$):

$$\begin{cases} u_{\mathrm{w}21}=\mathrm{sgn}\,(u_{21})\cdot\left(\tilde{U}_i-\gamma/2\right)=-0.5150, \\ u_{\mathrm{w}31}=\mathrm{sgn}\,(u_{31})\cdot\left(\tilde{U}_i+\gamma/2\right)=-0.5250. \end{cases} \tag{A6}$$

Here the condition $u_{\mathrm{w}31}<u_{\mathrm{w}21}$ holds true, indicating that the embedding bit is 0. Now, using these modified values, the watermarked image $\boldsymbol{A}_{\mathrm{w}}$ is obtained as

$$\boldsymbol{A}_{\mathrm{w}}=\boldsymbol{U}_{\mathrm{w}}\boldsymbol{S}\boldsymbol{V}^{\mathrm{T}}=\begin{bmatrix}70 & 47 & 26 & 134\\ 30 & 50 & 128 & 216\\ 53 & 242 & 7 & 97\\ 35 & 170 & 130 & 160\end{bmatrix}. \tag{A7}$$

The recipient of watermarked image $\boldsymbol{A}_{\mathrm{w}}$ will decompose the received image to extract the watermarking bits based on the conditions specified at the time of watermark embedding. The values extracted from $\boldsymbol{A}_{\mathrm{w}}$, based on the conditions, indicate that the watermarking bit is 1

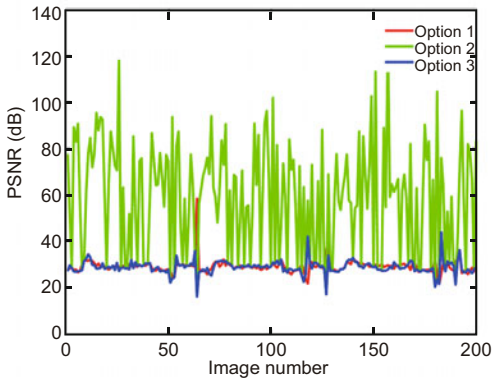

Fig. A1 Illustration of Finding 2

($u_{\mathrm{w}31}=-0.51\geq u_{\mathrm{w}21}=-0.52$), whereas in actuality the embedding bit is 0. To avoid this loss of information and false extraction, the elements of $\boldsymbol{V}$ are also involved in the watermark embedding process. The two values of $\boldsymbol{V}$ are modified as follows (for an embedding bit 0 and $\gamma=0.01$):

$$\begin{cases} v_{\mathrm{w}12}=\mathrm{sgn}\,(v_{12})\cdot\left(\tilde{V}-\gamma/2\right)=0.3050, \\ v_{\mathrm{w}13}=\mathrm{sgn}\,(v_{13})\cdot\left(\tilde{V}+\gamma/2\right)=0.3150. \end{cases} \tag{A8}$$

Now, using the modified $\boldsymbol{U}_{\mathrm{w}}$ and $\boldsymbol{V}_{\mathrm{w}}$, obtained from Eqs. (A6) and (A8) respectively, the watermarked image $\boldsymbol{A}_{\mathrm{w}}$ is obtained as

$$\boldsymbol{A}_{\mathrm{w}}=\boldsymbol{U}_{\mathrm{w}}\boldsymbol{S}\boldsymbol{V}_{\mathrm{w}}^{\mathrm{T}}=\begin{bmatrix} 43 & 47 & 26 & 134 \\ -3 & 50 & 128 & 216 \\ 85 & 242 & 7 & 97 \\ 44 & 170 & 130 & 160 \end{bmatrix}. \tag{A9}$$

To extract the watermarking bit, after decomposing $\boldsymbol{A}_{\mathrm{w}}$ using SVD, the condition is checked based on the elements of $\boldsymbol{U}_{\mathrm{w}}$. The left singular vector $\boldsymbol{U}_{\mathrm{w}}$ extracted from $\boldsymbol{A}_{\mathrm{w}}$ is

$$\boldsymbol{U}_{\mathrm{w}}=\begin{bmatrix} -0.31 & -0.16 & -0.77 & -0.53 \\ -0.50 & -0.66 & -0.05 & 0.56 \\ -0.53 & 0.74 & -0.19 & 0.37 \\ -0.61 & -0.02 & 0.60 & -0.52 \end{bmatrix}. \tag{A10}$$

It can been seen that $u_{31}=-0.53<u_{21}=-0.50$, which indicates that the embedding bit is 0. Hence, involving both left and right singular vectors in the watermark embedding process ensures robustness.